Title
Thermal Conductivity of Cementitious Composites Containing Microencapsulated Phase Change Materials

Author
Ricklefs, Alex

Publication Date
2016

Peer reviewed|Thesis/dissertation

University of California
Los Angeles

Thermal Conductivity of Cementitious Composites Containing Microencapsulated Phase Change Materials

A thesis submitted in partial satisfaction
of the requirements for the degree
Master of Science in Mechanical Engineering

by

Alex Ricklefs

2016

Abstract of the Thesis

Thermal Conductivity of Cementitious Composites Containing Microencapsulated Phase Change Materials

by

Alex Ricklefs

Master of Science in Mechanical Engineering

University of California, Los Angeles, 2016

Professor Laurent G. Pilon, Chair

This thesis investigates the effects of adding microencapsulated phase change materials (PCM) on the thermal conductivity of cement paste and cement mortar composites. Embedding cementitious composites with microencapsulated PCM has been considered a promising method for increasing the thermal mass of buildings to achieve greater energy efficiency. Cement paste and cement mortar samples were synthesized with a constant water to cement ratio of 0.45. Both contained microencapsulated PCM with diameter ranging from 17-20 μm, volume fraction up to 30%, and a melting temperature around 24°C. The cement mortar also contained quartz grains 150-600 μm in diameter such that the sum of the volume fractions of quartz and microencapsulated PCM was fixed at 55%. All samples were aged for more than 28 days. Their effective density and free moisture content were systematically measured. A guarded hot plate apparatus was designed, assembled, and validated according to the ASTM C177 to measure the effective thermal conductivity of the aged specimens of cement paste and cement mortar without and with microencapsulated PCM. Measurements were

performed between 10 and 40°C, encompassing the entire PCM phase change temperature window. The effective thermal conductivity of both the cement paste and the cement mortar composites was found to be nearly independent of temperature in the range considered. It also decreased as the volume fraction of microencapsulated PCM increased. Finally, excellent agreement was obtained between experimental data and the effective medium approximation derived by Felske (2004) for core-shell-matrix composites.

The thesis of Alex Ricklefs is approved.

Adrienne G. Lavine

Yungjie Hu

Laurent G. Pilon, Committee Chair

University of California, Los Angeles

2016

Table of Contents

List of Figures

List of Tables

Nomenclature

A_{gap}	area of the gap between the metered and guard heaters, mm^2
A_m	area of the metered heater, mm^2
c_p	specific heat, J/(kg·K)
e	thermal effusivity, $W \cdot s^{1/2}/(m^2 \cdot K)$
k	thermal conductivity, W/(m·K)
L_i	vertical distance between thermocouples in sample i, m
m	mass, g
$\dot{m}$	coolant mass flow rate, g/s
q_m	heat transfer rate from the metered heater, W
q_{loss}	estimated heat loss, W
$q_{w,i}$	heat transfer rate removed by cold plate i, W
q_i''	incoming heat flux in sample i, W/m^2
$\dot{Q}_i$	coolant volumetric flow rate, mL/min
R_g	resistance of the guard heater wire, Ω
R_m	resistance of the metered heater wire, Ω
$T_{j,i}$	temperature measured by thermocouple j in sample i, °C
U_g	voltage across the guard heater wire, V
U_m	voltage across the metered heater wire, V
V	volume, mm^3
w/c	water to cement mass ratio

Greek symbols

α	thermal diffusivity, m^2/s
Δx	associated systematic error in measurement x
ϕ_p	volume fraction of phase p in the cementitious composite

ϕ_{c+s}	volume fraction of microcapsules in the cementitious composite, $\phi_{c+s} = \phi_c + \phi_s$
$\phi_{c/s}$	volume fraction of core in the microcapsule, $\phi_{c/s} = \phi_c/(\phi_c + \phi_s)$
ϕ_w	free moisture content
ρ	density, g/cm^3

Subscripts

c	refers to core
$c + s$	refers to core-shell particle
$cold, i$	refers to the cold plate in contact with sample i
dry	refers to fully dry free moisture content
eff	refers to effective properties
i	refers to sample A or B
m	refers to matrix
q	refers to quartz sand
s	refers to shell
sat	refers to fully saturated free moisture content
w	refers to the chiller coolant
$w, 1, i$	refers to chiller coolant entering cold plate i
$w, 2, i$	refers to chiller coolant exiting cold plate i

ACKNOWLEDGMENTS

I would like to thank Professor Pilon for his direction and encouragement during my time at UCLA, Zander Thiele for all his help and guidance, and most importantly, my family for all the support they have given me over the years.

This study was supported in part by the California Energy Commission (Contract: PIR:-12-032). It does not necessarily represent the views of the Energy Commission, its employees, the State of California, or the National Science Foundation. The Energy Commission, the State of California, its employees, contractors, and subcontractors make no warranty, express or implied, and assume no legal liability for the information in this document; nor does any party represent that the use of this information will not infringe upon privately owned rights. This manuscript has not been approved or disapproved by the California Energy Commission nor has the California Energy Commission passed upon the accuracy or adequacy of the information in this report.

CHAPTER 1

Introduction

Embedding phase change materials (PCMs) in a concrete matrix has been proposed as a mean to improve building energy efficiency, and reduce the risk of thermal cracking [1–5]. PCMs achieve such beneficial actions by increasing the thermal mass (i.e., heat capacity) and thermal resistance by lowering the effective thermal conductivity of the cementitious composite materials [1–3]. Indeed, PCMs can store and release thermal energy in the form of latent heat through a reversible phase transition between solid and liquid states, actions which superimpose onto the sensible heat capacity of the concrete [6–9]. While numerous studies have quantified the benefits offered by enhanced thermal mass (i.e., sensible, and latent heat absorption and release), limited reports are available on the effect of PCM on the thermal conductivity of cementitious composites [1–3, 7, 10].

The thermophysical properties of cementitious composites, such as the heat capacity and thermal conductivity, are critical input variables required for modeling their thermal behavior and engineering performance for design purposes. For example, these properties determine the heat flow into and out of the building as well as the maximum and time lag in the building thermal load [11, 12]. In addition, it is important to understand the development of temperature and restrained stress gradients in cementitious composites to estimate the risk of thermal cracking [4, 5].

Therefore, to better understand how PCMs influence the thermal conductiv-

ity of cementitious composites, this paper quantifies the effect of incorporating microencapsulated PCM inclusions on the effective thermal conductivity of Type I ordinary Portland cement (OPC) pastes and mortars. A guarded hot plate apparatus was designed and fabricated, and its measurement performance rigorously validated. The thermal conductivity data acquired of microencapsulated PCM in cement pastes and mortars provides also experimental validation of effective medium approximation (EMAs) for three-phase cementitious composites containing cement paste, mineral aggregates (e.g., quartz inclusions), and functional inclusions (microencapsulated PCMs) [13].

CHAPTER 2

Background

2.1 Thermal conductivity measurement methods

Experimental methods available to measure the thermal conductivity of bulk solid materials can be categorized as either transient or steady-state. Transient methods include the plane source [14], hot strip [15], hot wire [16], hot bridge [17], and laser flash methods [18]. The first four methods involve temperature measurements collected over a time period ranging from 10 ns to 100 s during which the sample is heated [15–17]. A thin sensor is used to generate a pulse of thermal energy dissipated by the sample while simultaneously measuring the associated change in temperature at the sample surface [15–17]. The measured rate of thermal dissipation and change in sample temperature are used to calculate the thermal effusivity defined as $e = \sqrt{\rho c_p k}$ where ρ, c_p, and k are density, specific heat, and thermal conductivity of the sample, respectively [19]. The hot bridge method offers greater accuracy than the other three methods by using multiple sensors aligned in a Wheatstone bridge to collect sample surface temperature measurements with enhanced sensitivity [17]. Alternatively, the flash method [18] infers the thermal diffusivity α, defined as $\alpha = k/\rho c_p$. A pulse of thermal energy is applied to the front face of a parallel plane sample while the change in temperature on the back face is measured over a period of time [18]. The thermal diffusivity is then calculated based on the thickness of the sample and

the time required for the back surface to reach half of its maximum temperature measured over the duration of testing [18]. Since these transient methods do not measure thermal conductivity directly, uncertainty is introduced if the density ρ and specific heat c_p are not measured independently [20].

Steady-state methods, such as the hot plate and the guarded hot plate methods, measure the temperature difference across a sample maintained between a hot and a cold surface and subjected to one-dimensional (1D) steady-state heat conduction [21]. The thermal conductivity of the sample is determined from Fourier's law, based on the imposed heat flux and the measured temperature gradient across the sample [21, 22]. The hot plate method features simple measurement and analysis [21, 22]. However, radial heat losses in the hot plate make it difficult to achieve 1D steady-state conditions, thus introducing uncertainty in the measured thermal conductivity [21]. To mitigate these heat losses and to ensure 1D heat conduction, the guarded hot plate method includes a heated "guard" ring concentric to the center "metered" section of the heating element [21, 22]. The gap is filled with either air or a thermally insulating material to enhance radial thermal resistance around the hot plate. In addition, the guard ring is maintained at the same temperature as the metered section.

Overall, steady-state methods offer a direct measurement of thermal conductivity k, whereas transient methods require prior knowledge of the sample's density ρ and specific heat c_p. Steady-state methods are also simpler in terms of apparatus design and fabrication, experimental procedure, and data analysis [17]. However, they require longer experimental time than transient methods [14, 18, 23]. In this study, thermal conductivity measurements of cement paste and cement mortar containing microencapsulated PCM were performed using a guarded hot plate apparatus designed, fabricated, and validated per ASTM

C177-13 [23].

2.2 Thermal conductivity of cementitious composites

Table 2.1 summarizes the effective thermal conductivity reported in the literature for cement paste with different w/c ratio, age, and free moisture content ϕ_w, defined as the ratio of the volume of free water in a composite to its total volume of porosity [8, 24–29]. Most studies used one of the above-mentioned transient methods to measure the thermal conductivity. Xu and Chung [25] measured the thermal conductivity of Type I OPC paste samples with w/c of 0.45 using the laser flash method. More recently, Demirboga [27] measured the thermal conductivity of Type I OPC paste with a w/c of 0.35 using the hot wire method. Similarly, Bentz [24] measured the thermal conductivity of Type I OPC paste samples with w/c of 0.3 and 0.4 at 20°C using a transient plane source method. Table 2.1 indicates that measurements reported in these studies [24,25,27] differed by a factor of 2 although they considered similar samples. To the best of our knowledge, Demirboga [27] did not specify the sample temperature and specific heat while Bentz [24] did not specify the sample density. In addition, the specific heat of cement paste used by Xu and Chung [25] was 736 J/(kg·K) and almost half of that reported in the literature at 1530 J/(kg·K) [30]. This probably explains why the thermal conductivity reported by Xu and Chung [25] was almost half of that reported by Demirboga [27] and Bentz [24].

The effective thermal conductivity of cement paste has been shown to decrease as the water to cement mass ratio (w/c) increased [24]. This can be attributed to the enhanced pore formation within the composite with increasing amount of water [31]. The thermal conductivity of cement paste has also been observed to decrease by up to 30% over a 7-day hardening period but remained unchanged

beyond this period [32, 33]. The hardening process can take place in either water, ambient air, or humid air with up to 100% humidity [32, 33]. The thermal conductivity of cement paste was found to decrease significantly more when hardening occurred in ambient air [32] rather than submerged in water [33], when the pores are filled with air instead of water. Kim et al. [34] found that the thermal conductivity of cement paste at temperatures between 20-60°C decreased by up to 35% as the free moisture content ϕ_w decreased from 1 to 0. This can also be attributed to the difference in thermal conductivity between air and water filling up the pores [34].

Table 2.1: Thermal conductivity measurements reported in the literature for cement paste [24–27, 34].

w/c ratio	**Temp. (°C)**	**Age**	ϕ_w	**Method**	k_{eff} **(W/(m·K))**	**Ref.**
0.3	20°C	28 days	N/A	TPS	0.95-1.05	[24]
0.4	20°C	28 days	N/A	TPS	0.95-1.05	[24]
0.45	N/A	28 days	N/A	Laser flash	0.53	[25]
0.35	N/A	28 days	N/A	Laser flash	0.53	[26]
0.35	N/A	28 days	0	Hot wire	1.23	[27]
0.50	N/A	1 day	0.06	TPS	1.38	[32]
0.50	N/A	6 days	0.01	TPS	1.21	[32]
0.40	20°C	3 days	1	Hot wire	1.21	[34]
0.40	20°C	7 days	1	Hot wire	1.19	[34]
0.40	20°C	14 days	1	Hot wire	1.20	[34]
0.40	20°C	28 days	1	Hot wire	1.15	[34]
0.40	20°C	28 days	0	Hot wire	0.80	[34]
0.40	60°C	28 days	1	Hot wire	1.10	[34]
0.40	60°C	28 days	0	Hot wire	0.72	[34]

TPS: Transient plane source, N/A: Not specified

Moreover, the type and volume fraction of aggregates present in cement mortar composites can alter their effective thermal conductivity [26, 34, 35]. Table 2.2 summarizes the experimental studies reporting the thermal conductivity of cement mortar with different types and amount of aggregate inclusions as well as w/c ratio, age, and free moisture content ϕ_w [26, 29, 34]. For example, Uysal et al. [26] measured, by the hot wire method, the thermal conductivity of ce-

ment mortar containing pumice aggregate with a volume fraction ϕ_{agg} of up to 0.75. They found that the thermal conductivity was up to 46% lower than that of similar plain cement paste samples. This can be attributed to the fact that the pumice (a highly porous volcanic rock) has a lower thermal conductivity than cement paste [35]. It has also been reported that the effective thermal conductivity of cement mortar increased with increasing free moisture content ϕ_w [28, 29, 34, 36]. Jin et al. [36] measured the thermal conductivity of cement mortar with increasing free moisture content at 20°C using a transient plane source method. The thermal conductivity was found to increase by about 13% per degree of free moisture content over the range of 0 to 15% but increased by 2% per degree of free moisture content beyond [36]. Kim et al. [34] measured the thermal conductivity of fully saturated and dry cement mortar samples containing sand and stone aggregates made with different w/c ratio and aggregate volume fraction at temperatures between 20 - 60°C using a transient hot wire method. The effective thermal conductivity of these cement mortar samples was found to increase by up to 30% as the free moisture content ϕ_w increased from 0 (fully dry) to 1 (fully saturated) [34]. It also decreased by up to 16% as the sample temperature increased from 20°C and 60°C [34]. Additionally, the authors found very little change in the thermal conductivity of these samples over time when measured over a 28-day hardening period [34]. However, the conditions of the hardening process were not described. Overall, these results were consistent with the findings of previous studies [26, 28, 29, 36] and highlight the numerous factors that can affect the thermal conductivity of cementitious composites.

Table 2.2: Thermal conductivity measurements reported in the literature for cement mortar [26, 29, 34].

ϕ_{agg}	**w/c ratio**	**Temp.** (°C)	**Age**	ϕ_w	**Method**	k_{eff} **(W/(m·K))**	**Ref.**
N/A (sand)	0.35	N/A	28 days	N/A	Laser flash	0.58	[26]
0.38^{+}	0.65	18 - 35	N/A	0	Hot plate	1.25	[29]
0.38^{+}	0.65	18 - 35	N/A	1	Hot plate	1.94	[29]
0.3^{-}	0.65	18 - 35	N/A	0	Hot plate	1.30	[29]
0.3^{-}	0.65	18 - 35	N/A	1	Hot plate	2.08	[29]
0.29^{*}	0.65	18 - 35	N/A	0	Hot plate	2.56	[29]
0.29^{*}	0.65	18 - 35	N/A	1	Hot plate	4.39	[29]
0.7^{s}	0.40	20	28 days	1	Hot wire	2.47	[34]
0.7^{s}	0.40	40	28 days	1	Hot wire	2.50	[34]
0.7^{s}	0.40	60	28 days	1	Hot wire	2.30	[34]
0.7^{s}	0.40	20	28 days	0	Hot wire	1.97	[34]
0.7^{s}	0.40	40	28 days	0	Hot wire	1.94	[34]
0.7^{s}	0.40	60	28 days	0	Hot wire	1.84	[34]
0.35^{s}	0.40	20	28 days	1	Hot wire	1.71	[34]
0.35^{s}	0.40	40	28 days	1	Hot wire	1.74	[34]
0.35^{s}	0.40	60	28 days	1	Hot wire	1.64	[34]
0.35^{s}	0.40	20	28 days	0	Hot wire	1.28	[34]
0.35^{s}	0.40	40	28 days	0	Hot wire	1.27	[34]
0.35^{s}	0.40	60	28 days	0	Hot wire	1.15	[34]
0.25^{p}	N/A	N/A	28 days	0	Hot wire	1.35	[35]
0.50^{p}	N/A	N/A	28 days	0	Hot wire	1.17	[35]
0.50^{p}	N/A	N/A	28 days	0	Hot wire	1.05	[35]

Table 2.2: Thermal conductivity measurements reported in the literature for cement mortar [26, 29, 34].

ϕ_{agg}	**w/c ratio**	**Temp.** (°C)	**Age**	ϕ_w	**Method**	k_{eff} **(W/(m·K))**	**Ref.**
N/A[a]	N/A	20	4 days	0.84	TPS	0.4	[36]
N/A[a]	N/A	20	4 days	0.80	TPS	0.5	[36]
N/A[a]	N/A	20	4 days	0.76	TPS	0.5	[36]

[+]: quartz & dolerite, [−]: quartz & barytes, [*]: quartz & haematite, [s]: sand & stone

[p]: pumice, [a]: autoclaved aerated concrete, TPS: Transient plane source, N/A: Not specified

Finally, adding PCM to cementitious composites has been reported to decrease the effective thermal conductivity [8, 37, 38]. Table 2.3 and 2.4 summarize the studies reporting the thermal conductivity of cement mortar containing PCM either impregnated in the mortar or microencapsulated [8, 37, 38]. Both Xu and Li [37] and Zhang et al. [38] found that the thermal conductivity of cement mortar with impregnated PCM mass fraction up to 0.3 decreased linearly with increasing PCM mass fraction. Only Hunger et al. [8] has reported the experimentally measured thermal conductivity of concrete containing various volume fractions of *microencapsulated* PCM, as summarized in Table 2.4. The authors measured the thermal conductivity of self-compacting concrete containing up to 0.12 volume fraction (5 wt.%) of microencapsulated PCM between 19 and 28°C using the hot wire method. The specific heat and density of these samples were also measured independently. Unfortunately, the individual thermal conductivities and volume fractions of the PCM core and shell were not reported. Additionally, the study only measured self-compacting concrete. To the best of our knowledge, the thermal conductivity of other types of cementitious composites containing microencapsulated PCM has not been reported.

Table 2.3: Thermal conductivity measurements reported in the literature for cement mortar impregnated with PCM [37, 38].

ϕ^{+}_{agg}	ϕ_{c+s}	**w/c ratio**	**Temp. (°C)**	**Age**	ϕ_w	**Method**	k_{eff} **(W/(m·K))**	**Ref.**
0.2^{-}	0^{-}	0.5	N/A	28 days	N/A	TPS	2.06	[37]
0.2^{-}	0.1^{-}	0.5	N/A	28 days	N/A	TPS	1.82	[37]
0.2^{-}	0.2^{-}	0.5	N/A	28 days	N/A	TPS	1.56	[37]
0.2^{-}	0.3^{-}	0.5	N/A	28 days	N/A	TPS	1.35	[37]
0.2^{-}	0^{-}	0.5	N/A	N/A	N/A	TPS	2.19	[38]
0.2^{-}	0.012^{-}	0.5	N/A	N/A	N/A	TPS	1.97	[38]
0.2^{-}	0.017^{-}	0.5	N/A	N/A	N/A	TPS	1.90	[38]
0.2^{-}	0.025^{-}	0.5	N/A	N/A	N/A	TPS	1.85	[38]

$^{+}$: Non PCM aggregates, $^{-}$: Mass fraction (volume fraction not given)

TPS: Transient plane source, N/A: Not specified

Table 2.4: Thermal conductivity measurements reported in the literature for cement mortar containing embedded microencapsulated PCM [8].

ϕ^{+}_{agg}	ϕ_{c+s}	**w/c ratio**	**Temp. (°C)**	**Age**	ϕ_w	**Method**	k_{eff} **(W/(m·K))**	**Ref.**
0.63	0	0.45	19 - 28°C	28 days	N/A	Hot wire	3.4	[8]
0.61	0.025	0.45	19 - 28°C	28 days	N/A	Hot wire	2.9	[8]
0.57	0.077	0.45	19 - 28°C	28 days	N/A	Hot wire	2.3	[8]
0.57	0.124	0.45	19 - 28°C	28 days	N/A	Hot wire	2.1	[8]

$^{+}$: Non PCM aggregates, N/A: Not specified

2.3 Effective medium approximations

Several effective medium approximations (EMAs) have been proposed to predict the effective thermal conductivity of three-component core-shell-matrix composites such as cement paste with embedded microencapsulated PCM [13, 39–43]. For example, Felske [13] derived an EMA to predict the effective thermal conductivity of composites embedded with randomly distributed monodisperse spherical microcapsules. In absence of contact resistance at the shell-matrix interface, the effective thermal conductivity of three-component core-shell-matrix composites can be written as [13],

$$k_{eff} = \frac{2k_m(1-\phi_c-\phi_s)\left(3+2\frac{\phi_s}{\phi_c}+\frac{\phi_s k_c}{\phi_c k_s}\right)+(1+2\phi_c+2\phi_s)\left[(3+\frac{\phi_s}{\phi_c})k_c+2\frac{\phi_s k_s}{\phi_c}\right]}{(2+\phi_c+\phi_s)\left(3+2\frac{\phi_s}{\phi_c}+\frac{\phi_s k_c}{\phi_c k_s}\right)+(1-\phi_c-\phi_s)\left[(3+\frac{\phi_s}{\phi_c})\frac{k_c}{k_m}+2\frac{\phi_s k_s}{\phi_c k_m}\right]}. \tag{2.1}$$

Here, k and ϕ are the thermal conductivity and volume fraction and the subscripts c, s, and m refer to the core, shell, and matrix, respectively. Predictions of this model have been shown to agree very well with those based on detailed numerical simulations of spherical monodisperse and polydisperse core-shell-matrix particles ordered or randomly distributed in a continuous matrix. Wide ranges of constituent thermal conductivities and volume fractions were considered [44]. However, to the best of our knowledge, the Felske model [13] has not yet been validated against experimental measurements.

Moreover, the effective thermal conductivity of cementitious composites containing quartz sand and microencapsulated PCM could be determined using the EMA developed by Brailsford and Major [40] for two dissimilar spherical monodisperse homogeneous particles randomly distributed in a continuous matrix. Their

model is expressed as [40],

$$k_{eff} = \frac{k_m\phi_m + k_{c+s}\phi_{c+s}\dfrac{3k_m}{(2k_m + k_{c+s})} + k_q\phi_q\dfrac{3k_m}{(2k_m + k_q)}}{\phi_m + \phi_{c+s}\dfrac{3k_m}{(2k_m + k_{c+s})} + \phi_q\dfrac{3k_m}{(2k_m + k_q)}}, \tag{2.2}$$

where ϕ_{c+s} and k_{c+s} are the volume fraction and the effective thermal conductivity of the core-shell particles and ϕ_q and k_q are those of quartz sand grains. In addition, the effective thermal conductivity k_{c+s} of the core-shell particles could be predicted by a model developed by Park et al. [39] and expressed as

$$k_{c+s} = \frac{2(1-\phi_{c/s})k_s + 2(1+2\phi_{c/s})k_c}{(2+\phi_{c/s})k_s + (1-\phi_{c/s})k_c}k_s, \tag{2.3}$$

where $\phi_{c/s} = \phi_c/(\phi_c + \phi_s)$ is the volume fraction of the core with respect to that of the shell. Note that Equation (2.3) is just one part of an EMA developed by Park et al. [39] to predict the effective thermal conductivity of core-shell-matrix composites. In its full form, the Park model [39] is equivalent to the Felske model [13] given by Equation (2.1) and neglecting the thermal contact resistance.

The present study aims to measure the effective thermal conductivity of cement paste and cement mortar without and with microencapsulated PCM for volume fraction ϕ_{c+s} ranging from 0 to 0.3 and temperature between 10 and 40°C using the guarded hot plate method. The experimentally measured thermal conductivity values were compared with predictions by the Felske model [13] for cement paste microencapsulated PCM composites and the combination of the models proposed by Brailsford and Major [40] and Park [39] for cement mortar microencapsulated PCM composites. Once validated against experimental data, these EMAs could be used for the thermal design of cementitious PCM composites for various applications.

CHAPTER 3

Experiments

3.1 Materials and methods

3.1.1 Sample synthesis

Two types of cementitious samples were investigated in this study, namely cement paste and cement mortar, each without and with microencapsulated PCM. The cementitious composite samples were prepared as per ASTM C305 [45]. Cement paste samples were made using Type I ordinary Portland cement (OPC) mixed with deionized (DI) water at a constant w/c ratio of 0.45. Water-reducing admixture (Glenium 7500, BASF Corporation) was added up to 2% of the cement paste mass to improve the fluidity of the mixture. The PCM microcapsules (MPCM24D, MicroTek Laboratories Inc) consisted of a polymeric melamine-formaldehyde shell (10-15 mass %) surrounding a paraffinous core (85-90 mass %) with a melting temperature around 24°C [46]. The microcapsules featured a mean outer particle diameter of 17-20 μm [47] and an effective density of 900 kg/m^3 [46]. The PCM microcapsules volume fraction ϕ_{c+s} in the cement paste ranged from 0 to 0.3 in 0.1 increments. Cement mortar samples were synthesized by adding quartz sand (U.S. Silica Company) to the cement paste. The ASTM graded quartz sand was graded between 600 μm and 150 μm sieves, with 96-100% passing through the 600 μm sieve and 0-4% passing through the 150 μm sieve [48].

The quartz has a reported density of 2650 kg/m^3 [49]. The PCM microcapsule volume fraction ϕ_{c+s} in cement mortar ranged from 0 to 0.2 in 0.1 increments. The volume fractions of graded quartz sand ϕ_q and of PCM microcapsules ϕ_{c+s} in the mortar samples were such that their sum $\phi_q + \phi_{c+s}$ was kept constant and equal to 0.55.

The cementitious composite samples were cast into a cylindrical acrylic mold 38 mm in height and 50.8 mm in inner diameter. The samples were cured in sealed humid conditions for 24 hours. After initial curing, the samples were removed from the mold and the top and bottom of the sample were finished manually with 600 grit sand paper. All samples were aged in ambient air at room temperature and an average relative humidity around 60% for 28 days to ensure that they had fully hardened and featured a stable microstructure [32, 33]. Samples were synthesized in duplicates since the guarded hot plate method requires two identical samples to perform the thermal conductivity measurements. In order to measure the thermal conductivity k_{eff}, two radial holes were drilled to embed two thermocouples along the vertical axis of each aged sample, separated by an axial distance L of around 25 mm. Thermal cement (Arctic Alumina) with a thermal conductivity around 1 W/(m·K) was used to fix the thermocouples in place and achieve good thermal contact with the composite material.

3.1.2 Density measurements

The effective density ρ_{eff} of the cementitious composite samples was determined by measuring their volume V and their mass m independently, i.e., $\rho_{eff} = m/V$. These measurements were performed after the samples had aged for 28 days. The effective density of a few plain cement paste and mortar samples was also measured daily during the hardening and aging processes to determine the sample

age beyond which the density remained constant. Moreover, once the thermal conductivity measurements were performed, the density of each sample investigated was measured for oven dry and fully saturated moisture conditions. To achieve a fully dry state, samples were dried at 105°C in a sealed oven for 24 h [28]. To achieve a fully saturated state, they were submerged in boiling DI water for 5 h [28]. Then, the free moisture content ϕ_w in the aged samples of effective density ρ_{eff} was determined from the measured densities of fully dry ρ_{dry} and fully saturated ρ_{sat} samples according to [36, 50],

$$\phi_w = \frac{\rho_{eff} - \rho_{dry}}{\rho_{sat} - \rho_{dry}}. \tag{3.1}$$

3.1.3 Guarded hot plate apparatus

To measure the thermal conductivity of the cementitious composite specimens, a guarded hot plate apparatus was designed and fabricated in accordance with ASTM C177-13 [23]. Figure 3.1 illustrates the entire experimental setup including (i) the guarded hot plate test section, (ii) a cooling/heating recirculating chiller (Polystat, Cole-Parmer), (iii) two flow meters (FLR-1009, Omega), (iv) two variable DC power generators (Dual DC power supply, Beckman Industrial), (v) two 10-channel data acquisition board (DAQ) (OMB-DAQ-56, Omega), and (vi) a personal computer. The guarded hot plate method require two identical samples denoted by A and B. Each sample was secured between custom-made hot and cold plates. A vertical clamp was used to hold the test section together and to ensure good thermal contact between the samples and the hot and cold plates. The entire test section was wrapped in 5 cm thick microporous insulation (Cerablanket, Morgan Thermal Ceramics) with a thermal conductivity of 0.07 W/(m·K) and a density of 64 kg/m^3 to reduce heat losses [51]. The cold plates were connected to the recirculating chiller by flexible pipes directing the chiller

coolant in and out of each cold plate. The volumetric flow rate $\dot{Q}_A$ and $\dot{Q}_B$ of the coolant into each cold plate were measured by a digital flow meter attached to each inlet pipe. Each DAQ input had a built-in cold-junction for reference measurements. DASYlab software was used to record the data.

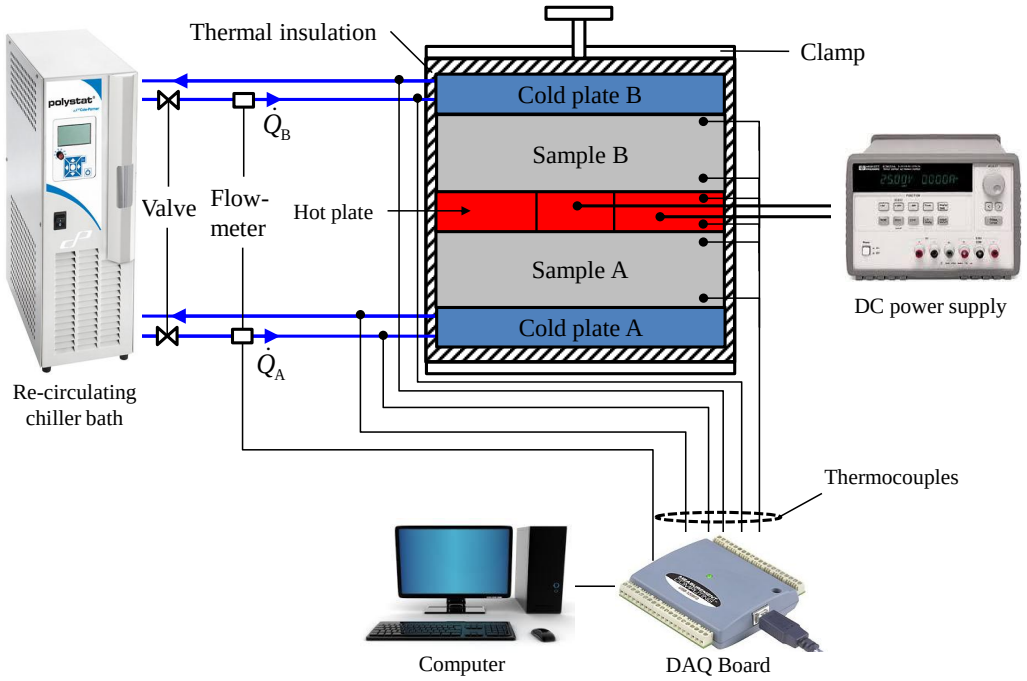

Figure 3.1: Experimental setup used to measure the effective thermal conductivity of cementitious PCM composites based on the guarded hot plate method.

Figure 3.2 shows details of the guarded hot plate test section, consisting of a hot plate and two cold plates separated by two identical samples A and B. The hot plate assembly consisted of a metered heater and of a concentric guard heater, separated by a 0.25 mm gap. The temperatures (i) $T_{1,A}$, $T_{2,A}$,$T_{1,B}$, and $T_{2,B}$ within samples A and B, (ii) $T_{m,A}$ and $T_{m,B}$ at the bottom and top faces of the metered heater in contact with samples A and B, (iii) $T_{g,A}$ and $T_{g,B}$ at

the bottom and top faces of the guard heater, and (iv) $T_{cold,A}$ and $T_{cold,B}$ at the center of the cold plates were measured using type-T copper-constantan 24 gage thermocouples connected to the DAQ boards. The temperature differences $T_{w,2,A}$-$T_{w,1,A}$ as well as $T_{w,2,B}$-$T_{w,1,B}$ of the coolant between the outlet and inlet of cold plates A and B, respectively, were also measured by type-T thermocouples to reduce uncertainty by using the inlet coolant temperature as the thermocouple reference junction. First, each thermocouple was calibrated by immersing it in a circulating water bath held at a constant and known temperature between 10 and 40°C with 5°C increments. The thermocouple voltage was fitted as a linear function of voltage for each individual thermocouple and the fit was used in the data acquisition software.

Figure 3.3 shows top- and side-views of (a,b) the metered heater and (c,d) guard heater along with their respective dimensions. The guard section outer diameter was 50.8 mm and corresponded to the maximum sample diameter, as described in ASTM C177-13 [23]. Both metered and guard heaters were fabricated using copper for its large thermal conductivity ensuring uniform temperature over the hot plate surfaces. Resistance heating 22 gauge nichrome-60 wires were embedded in 0.8 mm deep circular grooves machined at the top of both heaters, as illustrated in Figures 3.3a and 3.3c. The wires were held in place using electrically insulating thermal cement (Arctic Alumina). Then, a 1.8 mm thick copper lid was attached to the top of each heater using thermal cement (Arctic Alumina) to cover the heating wires and provide a planar surface in contact with the samples. The electric resistances R_m and R_g of the heating wires in the metered and guard heaters were measured with a digital multimeter (34401A, Agilent) during each thermal conductivity measurement after reaching steady-state. Resistances R_m and R_g ranged between 0.225 and 2.450 Ω and 0.614 and 6.688 Ω respectively for heater temperatures between 10 and 40°C. Each heater was heated by Joule

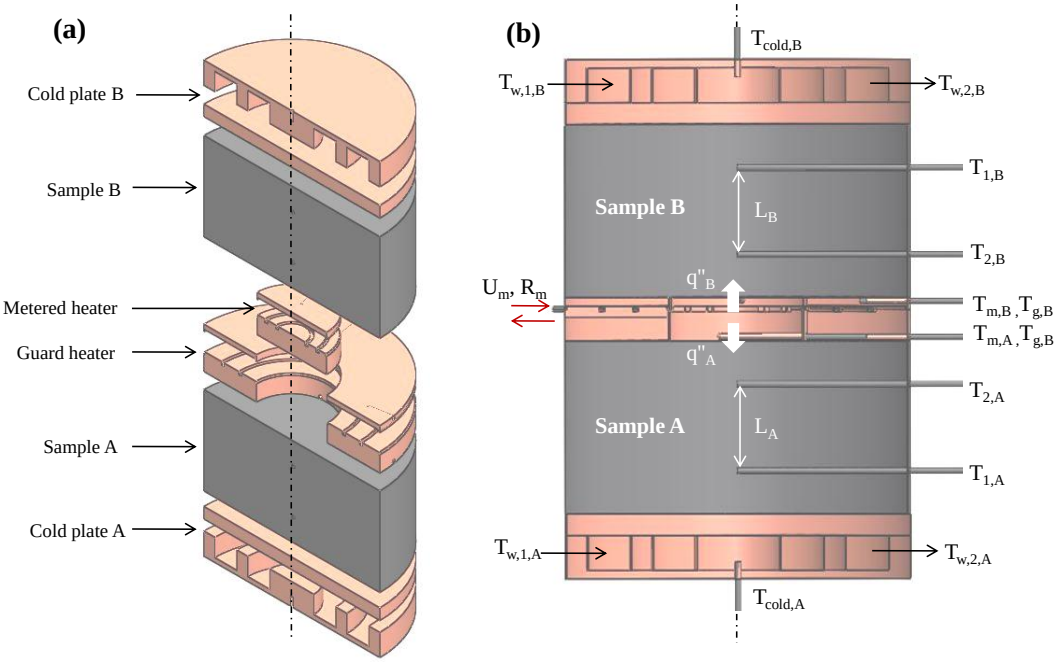

Figure 3.2: (a) Exploded cross-sectional view of the guarded hot plate test section labeling each component and (b) collapsed cross-sectional view detailing thermocouple locations and relevant notations.

heating in the wire connected to a DC power supply. The voltages U_m and U_g across each wire were adjusted until the temperature of the metered and guard heaters were identical within $\pm 0.3^{\circ}$C, per ASTM C177-13 [23]. Voltages U_m and U_g were also measured with a digital multimeter and ranged from 0.236 to 1.180 V and from 1.140 to 2.550 V, respectively. At steady-state, the thermal energy U_m^2/R_m dissipated in the hot plate was evenly distributed between samples A and B and ranged between 0.18 and 0.68 W.

Figure 3.4 shows the top- and side-views of the two identical cold plates along with their dimensions. The cold plate assembly consisted of a hollowed disc, 50.8 mm in diameter, made of copper with inlet and outlet copper tubes welded on

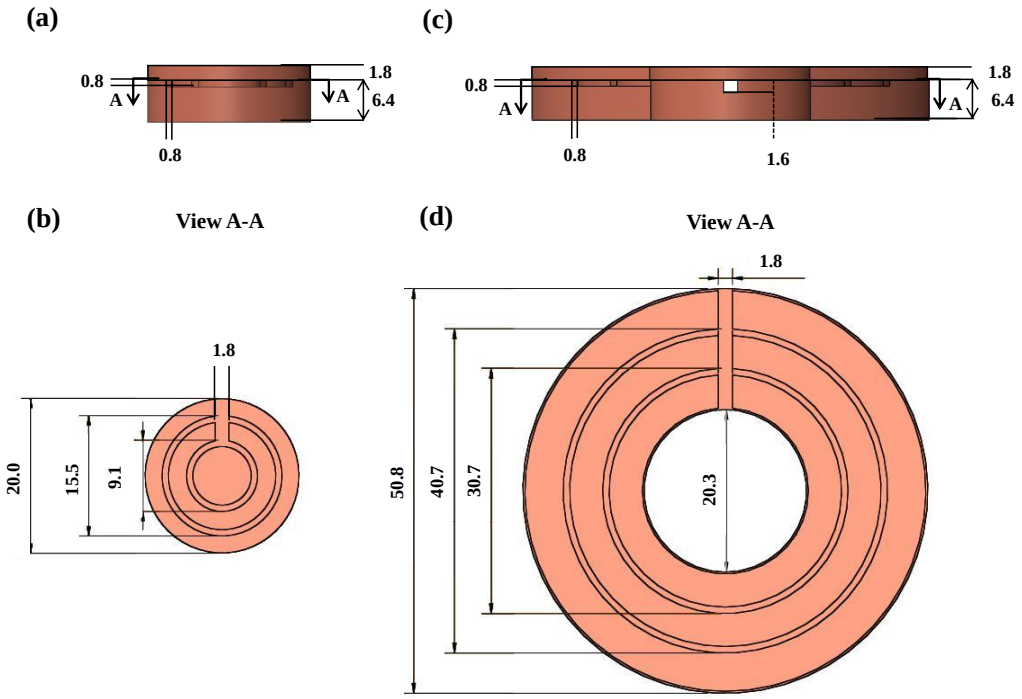

Figure 3.3: Side and top-views of the metered (a) and (b) and guard (c) and (d) sections, respectively, along with their associated dimensions (all in mm).

diametrically opposite sides. Internal baffles were machined 5.1 mm in depth to direct the coolant around the cold plate to ensure isothermal conditions over the entire outer plate surface. A 1.8 mm thick copper disc was then welded on top to properly seal the cold plate. The inlet and outlet copper tubes had an inner and outer diameter of 5.0 and 6.4 mm, respectively. The bottom and top cold plates, respectively in contact with samples A and B, were maintained at approximately the same temperature by manually adjusting the coolant volumetric flow rates $\dot{Q}_A$ and $\dot{Q}_B$ through each plate via individual valves. These flow rates ranged between 100 and 500 mL/min depending on the cold bath coolant and temperature and on the desired cold plate temperature. Water and water-glycol mixture were used

as the coolant for thermal conductivity measurements at cold plate temperatures above and below 10°C, respectively.

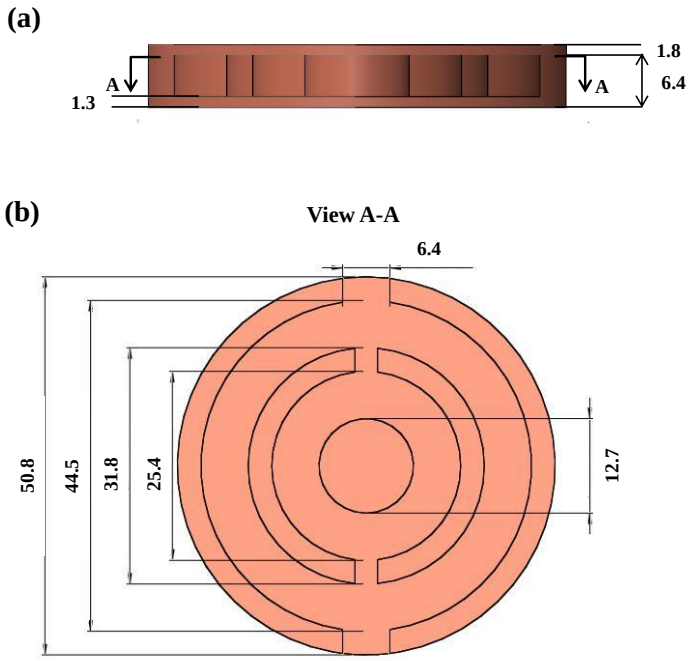

Figure 3.4: Side (a) and top (b) view of the cold plate with its associated dimensions (all in mm).

3.2 Experimental methodology

3.2.1 Data analysis

The effective thermal conductivity of sample i was calculated using Fourier's law given by

$$k_i(\bar{T}) = \frac{q_i L_i}{A(T_{2,i} - T_{1,i})} \qquad \text{with } i = \text{A or B} \tag{3.2}$$

where q_i is the heat transfer rate (in W/m) through sample i and L_i is the distance separating the thermocouples measuring $T_{1,i}$ and $T_{2,i}$. Here, A is the effective surface area of the metered heater as defined by ASTM C177-13 [23] and given by $A = A_m + A_{gap}/2$, where A_m and A_{gap} are the surface areas of the metered heater and gap section, respectively. The thermal conductivity $k_i(\bar{T})$ was estimated as the average temperature $\bar{T} = (T_{1,i} + T_{2,i})/2$. Under steady-state conditions, the heat transfer rate q_i was estimated as the average of the measured heat input from the guarded hot plate and of the heat removed from the cold plate i, i.e.,

$$q_i = \frac{1}{2}(q_m + q_{w,i}) \tag{3.3}$$

where q_m and $q_{w,i}$ are the heat transfer rates measured on each side of the sample. The heat transfer rate q_m from the guarded hot plate can be estimated from the measured voltage U_m and resistance R_m across the metered heater as $q_m = U_m^2/2R_m$. The heat transfer rate $q_{w,i}$ removed by the cold plate on one side of the sample is expressed as $q_{w,i} = \dot{m}_i c_{p,w} (T_{w,2,i} - T_{w,1,i})$, where $c_{p,w}$ is the specific heat of the coolant and ($T_{w,2,i}$-$T_{w,1,i}$) is the coolant temperature difference measured between the outlet and inlet of the cold plate i. The mass flow rate $\dot{m}_i$ was determined by $\dot{m}_i = \rho_w \dot{Q}_i$, where $\dot{Q}_i$ is the volumetric flow rate measured by the digital flow meter and ρ_w is the density of the coolant at 10°C, taken as 999.8 kg/m^3 [30] and 1345 kg/m^3 [52] for water and water-glycol, respec-

tively. The specific heat $c_{p,w}$ at 10°C was taken as 4.19 kJ/(kg·K) [30] and 2.68 kJ/(kg·K) [52] for water and water-glycol, respectively. Finally, the temperature measurements of $T_{1,i}$ and $T_{2,i}$ in samples A and B were averaged over 30 minute intervals to determine the thermal conductivities k_A and k_B of samples A and B. Then, the effective thermal conductivity of the cementitious composite sample was estimated as

$$k_{eff}(T) = \frac{1}{2}\left(\bar{k}_A + \bar{k}_B\right) \text{ with } \bar{k}_i(\bar{T}) = \frac{1}{n}\sum_{j=1}^{n} k_i(j) \tag{3.4}$$

where n is the total number of measurements of $k_A(j)$ and $k_B(j)$. A minimum of four consecutive measurements of k_A and k_B were performed, as required per ASTM C177-13 [23].

3.2.2 Operation and procedure

Measurements were performed once samples had aged for at least 28 days. First, identical samples A and B instrumented with thermocouples were places in the test section and the clamp was tightened. The power generators connected to the resistance heating wires were then turned on and the voltages U_m and U_g were adjusted until the metered and guard heaters reached steady-state temperatures falling within ±0.3°C of each other. Meanwhile, the recirculating chiller was set to the desired cold plate temperature. The flow rates $\dot{Q}_A$ and $\dot{Q}_B$ to the cold plates were then adjusted until both cold plates A and B had temperatures within ±0.3°C of one another. Steady-state conditions were considered to be reached when the temperatures of the hot and cold plate surfaces did not fluctuate by more than 0.3°C over three 30 minute intervals [23]. Then, the temperatures $T_{1,A}$ and $T_{2,A}$ in sample A and $T_{1,B}$ and $T_{2,B}$ in sample B were recorded and averaged over 30 minute intervals [23]. A single measurement of effective thermal conductivity $\bar{k}_A$ and $\bar{k}_B$ at a given temperature lasted about 8 hours, corresponding to the time

for the apparatus to reach steady-state and to record at least four consecutive measurements of k_A and k_B.

3.2.3 Experimental uncertainty

The uncertainty in the thermal conductivity measurement of sample i depended on the systematic error in the measurements of q_i, A, L_i, $T_{1,i}$, and $T_{2,i}$. Based on Equation (3.2), it was expressed as,

$$\frac{\Delta k_i}{k_i} = \left[\left(\frac{\Delta q_i}{q_i} \right)^2 + \left(\frac{\Delta A}{A} \right)^2 + \left(\frac{\Delta L_i}{L_i} \right)^2 + \frac{\Delta T_{2,i}^2 + \Delta T_{1,i}^2}{\left(T_{2,i} - T_{1,i} \right)^2} \right]^{1/2} \tag{3.5}$$

where Δx is the systematic error associated with variable x. The experimental uncertainty associated with q_i was due to heat losses through the samples, resistance between the sample and the hot and cold plates, and heat losses through the gap [53, 54]. It can be written as,

$$\frac{\Delta q_i}{q_i} = \left[\left(\frac{\Delta q_m}{q_m} \right)^2 + \left(\frac{\Delta q_{w,i}}{q_{w,i}} \right)^2 + 2\frac{\sigma_q^2}{q_i^2} \right]^{1/2} . \tag{3.6}$$

Here, σ_q denotes the standard deviation of the heat transfer rate q_i with variance σ_q^2 estimated as ,

$$\sigma_q^2 = \frac{1}{2} \left(\frac{q_{loss,i}}{2} \right)^2 . \tag{3.7}$$

The heat loss $q_{loss,i}$ for sample i can be estimated as the difference between the heat input $q_m = U_m^2/2R_m$ supplied by the hot plate to each sample and the heat transfer rate $q_{w,i} = \dot{m}_i c_{p,w} \left(T_{w,2,i} - T_{w,1,i} \right)$ carried by the coolant passing through the cold plate, i.e.,

$$q_{loss,i} = \frac{1}{2} \frac{U_m^2}{R_m} - \dot{m}_i c_{p,w} \left(T_{w,2,i} - T_{w,1,i} \right) . \tag{3.8}$$

The uncertainties associated with q_m and $q_{w,i}$ are expressed as,

$$\left(\frac{\Delta q_m}{q_m} \right)^2 = \left(2\frac{\Delta U_m}{U_m} \right)^2 + \left(\frac{\Delta R_m}{R_m} \right)^2 \tag{3.9}$$

and

$$\left(\frac{\Delta q_{w,i}}{q_{w,i}}\right)^2 = \left(\frac{\Delta \dot{Q}_i}{\dot{Q}_i}\right)^2 + \left(\frac{\Delta \rho_w}{\rho_w}\right)^2 + \left(\frac{\Delta c_{p,w}}{c_{p,w}}\right)^2 + \left(\frac{\Delta (T_{w,2,i} - T_{w,1,i})}{T_{w,2,i} - T_{w,1,i}}\right)^2. \tag{3.10}$$

The uncertainty in voltage ΔU_m and resistance ΔR_m correspond to the measurement uncertainty from the digital multimeter and were on the order of ± 0.001 V and ± 0.001 Ω. The uncertainty in the coolant volumetric flow rate $\Delta \dot{Q}_i$ was on the order of ± 1 mL/min based on the manufacturer calibration. The coolant density ρ_w and specific heat $c_{p,w}$ were taken as constant values, they had uncertainties $\Delta \rho_w$ of 10 kg/m^3 and $\Delta c_{p,w}$ of 0.05 kJ/(kg·K) due to fluctuations in the coolant temperature. The uncertainty in the axial distance between the two thermocouples in each sample ΔL_i was on the order of ± 0.5 mm. Thermal expansion was deemed to be negligible given the small difference between the temperatures at which thermal conductivity and the distance L_i were measured [55, 56]. The uncertainty ΔA was estimated as $\Delta A = \Delta A_m + 1/2 \Delta A_{gap}$, where uncertainties ΔA_m and ΔA_{gap} in the surface area measurements were on the order of ± 0.5 mm^2. On completion of the thermocouple calibration procedure, the uncertainty in temperature measurements $\Delta T_{2,i}$, $\Delta T_{1,i}$, and $\Delta (T_{w,2,i} - T_{w,1,i})$ were on the order of $\pm 0.5^{\circ}$C. The heat loss $q_{loss,i}$, given by Equation (3.8), was the main contribution to the experimental uncertainty $\Delta q_i / q_i$ and represented 10-20% of the averaged heat input q_m. The uncertainty terms for the sample and coolant temperature measurements and the heat loss were also major sources of error. Thus, the test section was carefully insulated and large temperature differences $(T_{2,i} - T_{1,i})$ across the sample and $(T_{w,2,i} - T_{w,1,i})$ across the cold plate were imposed to reduce uncertainty.

Finally, uncertainty in the measured effective thermal conductivity k_{eff} of the

cementitious composite materials of samples A and B was expressed as

$$\frac{\Delta k_{eff}}{k_{eff}} = \sum_{j=1}^{n} \frac{1}{2n} \left[\Delta k_A(j)^2 + \Delta k_B(j)^2 + 2cov(k_A(j), k_B(j))\right]^{1/2} \tag{3.11}$$

where Δk_A and Δk_B are determined from Equations (3.5) to (3.10) while $cov(k_A(j), k_B(j))$ is the covariance of k_A and k_B defined as,

$$cov(k_A, k_B) = \frac{(k_A(j) - \bar{k}_A)(k_B(j) - \bar{k}_B)}{n}. \tag{3.12}$$

This covariance term was used to account for the deviation of the different measurements of k_A and k_B from their respective mean $\bar{k}_A$ and $\bar{k}_B$, respectively. In practice, measurements of $k_A(j)$ and $k_B(j)$ were highly repeatable. Intersample variability, accounted for by $cov(k_A, k_B)$, led to an average difference between $k_A(j)$ and $k_B(j)$ of 0.15 W/(m·K). The experimental uncertainty in k_{eff} was mainly due to uncertainties in temperature measurements $\Delta T_{1,i}$, $\Delta T_{2,i}$, and $\Delta\left(T_{w,2,i} - T_{w,1,i}\right)$.

3.2.4 Validation

In order to validate the guarded hot plate apparatus, the experimental methodology, and the data analysis described in the previous sections, the thermal conductivity of two certified reference material (CRM) Pyrex 7740 glass cylindrical samples (Corning 7740, Esco Optics) was measured. The samples were 38 mm in thickness and 50.8 mm in diameter. Their thermal conductivity k_p (in W/(m·K)) was known as a function of temperature, with ±6.5% uncertainty, between -75 and 195°C and expressed as [57],

$$k_p = 1.1036 + 1.659 \times 10^{-3}T - 3.982 \times 10^{-5}T^2 + 6.764 \times 10^{-9}T^3 \tag{3.13}$$

where T is the sample temperature (in °C).

Figure 3.5 compares the experimentally measured thermal conductivity of Pyrex glass with predictions by Equation (3.13) for temperature ranging from 10 to 40°C. The error bars illustrate the systematic and random error associated with each measurement estimated by Equation (3.5). It is evident that the experimentally measurements agreed, within experimental uncertainty, with predictions by Equation (3.13) over the entire temperature range considered. These results established that the guarded hot plate apparatus, experimental methodology, and the data analysis were valid and could be used to accurately measure the thermal conductivity of cementitious composite samples.

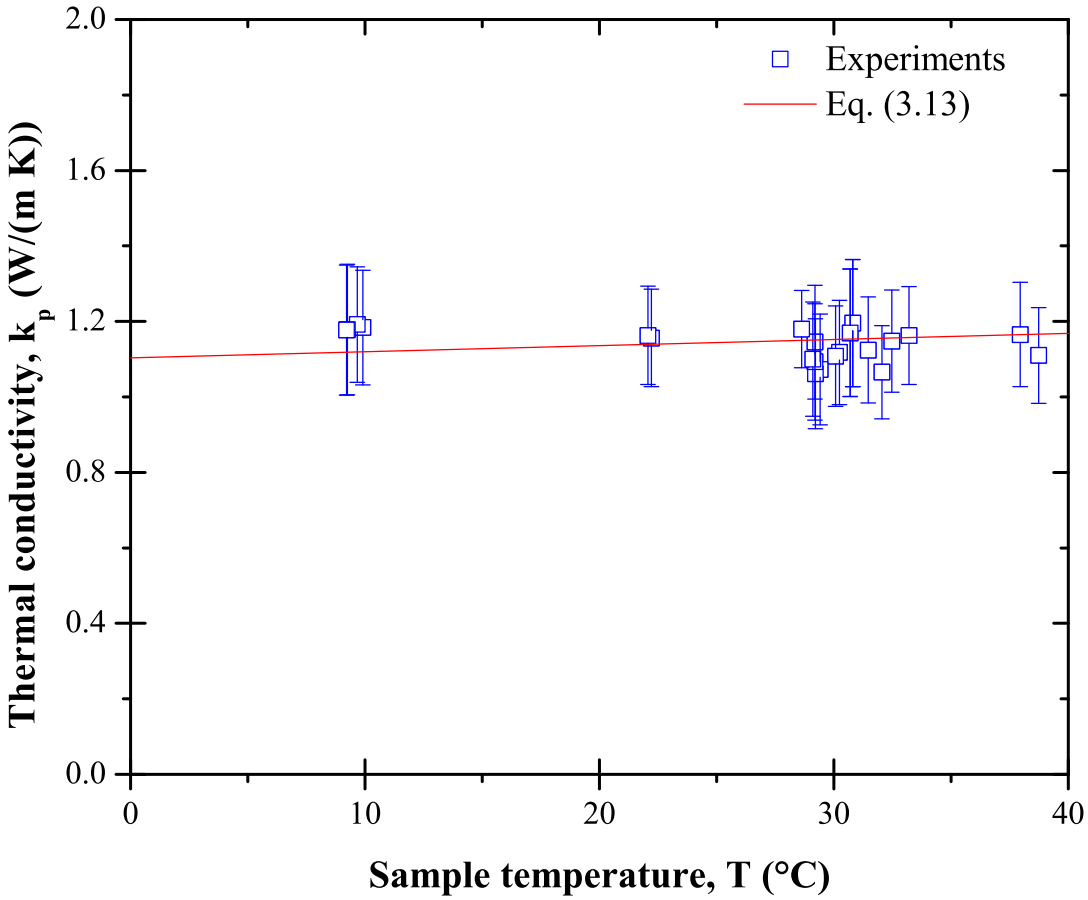

Figure 3.5: Measured thermal conductivity of Pyrex glass and the reported thermal conductivity of the Pyrex certified reference material BCR-039 given by Equation (3.13) [57].

CHAPTER 4

Results and Discussion

4.1 Sample density and free moisture content

Figure 4.1 shows the measured density of two cement mortar samples with volume fraction ϕ_q of graded quartz sand of 0.35 and 0.45 but without microencapsulated PCM, as a function of time over a 28 day hardening period. It demonstrates that density decreased significantly during the first 4 days and remained constant after 20 days.

Table 4.1 summarizes (i) the effective density ρ_{eff}, (ii) the dry ρ_{dry} and (iii) saturated ρ_{sat} effective densities, as well as (iv) the free moisture content ϕ_w measured for each samples aged more than 28 days. It indicates that the free moisture content of the cement paste-PCM composite samples was around 0.2 - 0.4 while that of the cement mortar-PCM composite samples was less than 0.1. This difference could be attributed to the fact that the graded quartz sand does not absorb water.

4.2 Cement paste with microencapsulated PCM

Figure 4.2a plots the thermal conductivity of cement paste containing microencapsulated PCM with volume fraction ϕ_{c+s} of 0, 0.1, 0.2, and 0.3 as a function of temperature between 10 and 50°C. The error bars correspond to the systematic

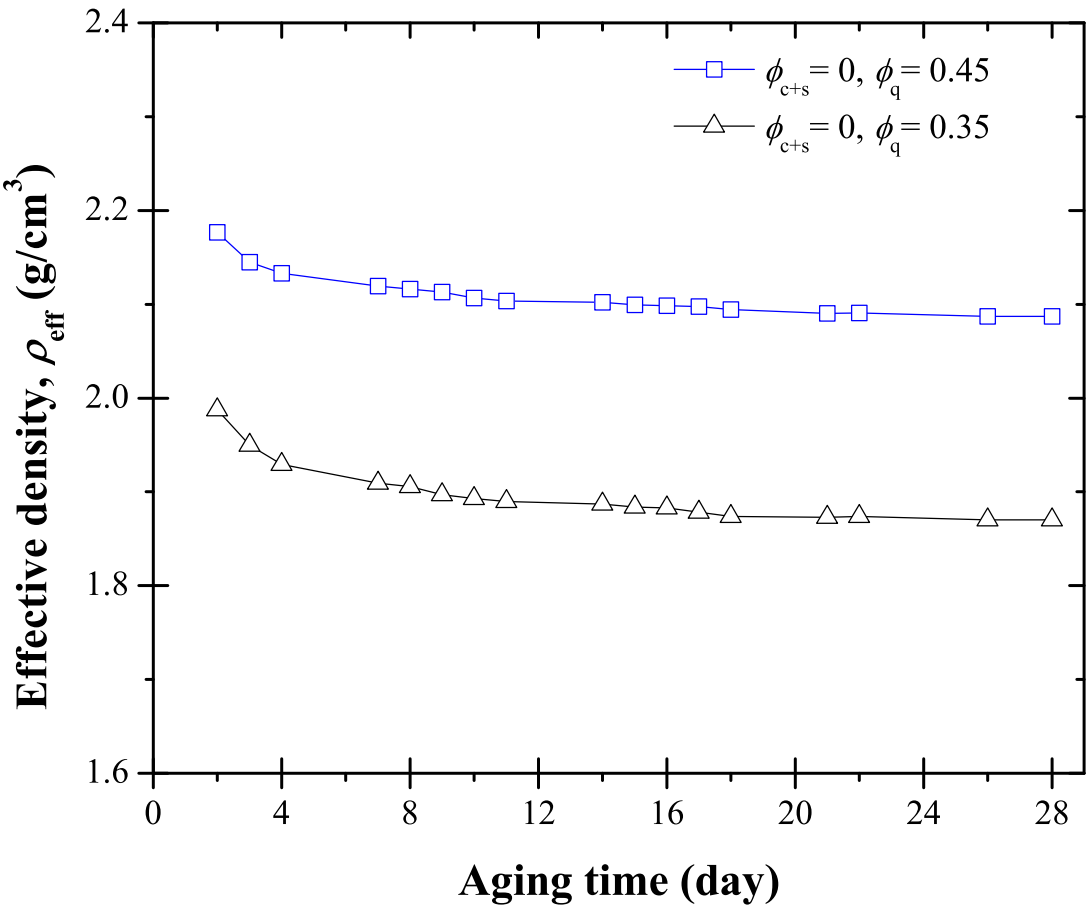

Figure 4.1: Effective density ρ_{eff} of cement mortar containing graded quartz sand with volume fraction ϕ_q of 0.45 and 0.35 but no microencapsulated PCM (ϕ_{c+s}=0) over a 28 day hardening period.

and random error associated with each measurement, as estimated by Equation (3.11). It indicates that the thermal conductivity of each specimen was nearly independent of temperature between 10 and 50°C. In addition, this temperature range encompassed the entire phase change temperature window of the PCM [47]. This indicates that the thermal conductivity was not affected appreciably by the occurrence of phase change, unlike the effective specific heat [47]

Figure 4.2b plots the temperature-averaged effective thermal conductivity

$<k_{eff}>$ of cement paste-PCM composite specimens as a function of microencapsulated PCM volume fraction ϕ_{c+s} ranging from 0 to 0.3. It indicates that the average effective thermal conductivity $<k_{eff}>$ decreased almost linearly as the microencapsulated PCM volume fraction ϕ_{c+s} increased. This can be attributed to the fact that the thermal conductivity of both the PCM core and shell was smaller than that of cement paste. Figure 4.2b also shows predictions by the Felske model [13], given by Equation (2.1), using the thermal conductivity of plain cement paste (i.e., $\phi_{c+s} = 0$) measured as 1.20±0.13 W/(m·K) as the matrix thermal conductivity $<k_m>$. In addition, the thermal conductivity of the MPCM24D core k_c was taken as 0.21 W/(m·K) [46, 58] and that of the shell k_c as 0.42 W/(m·K) near room temperature [59]. Figure 4.2b indicates that predictions by the Felske model [13] agreed well with experimental measurements. The relative difference was less than 4.5%. Table 4.1 summarizes the effective thermal conductivity $<k_{eff}>$ for each composition averaged over the temperature ranged considered.

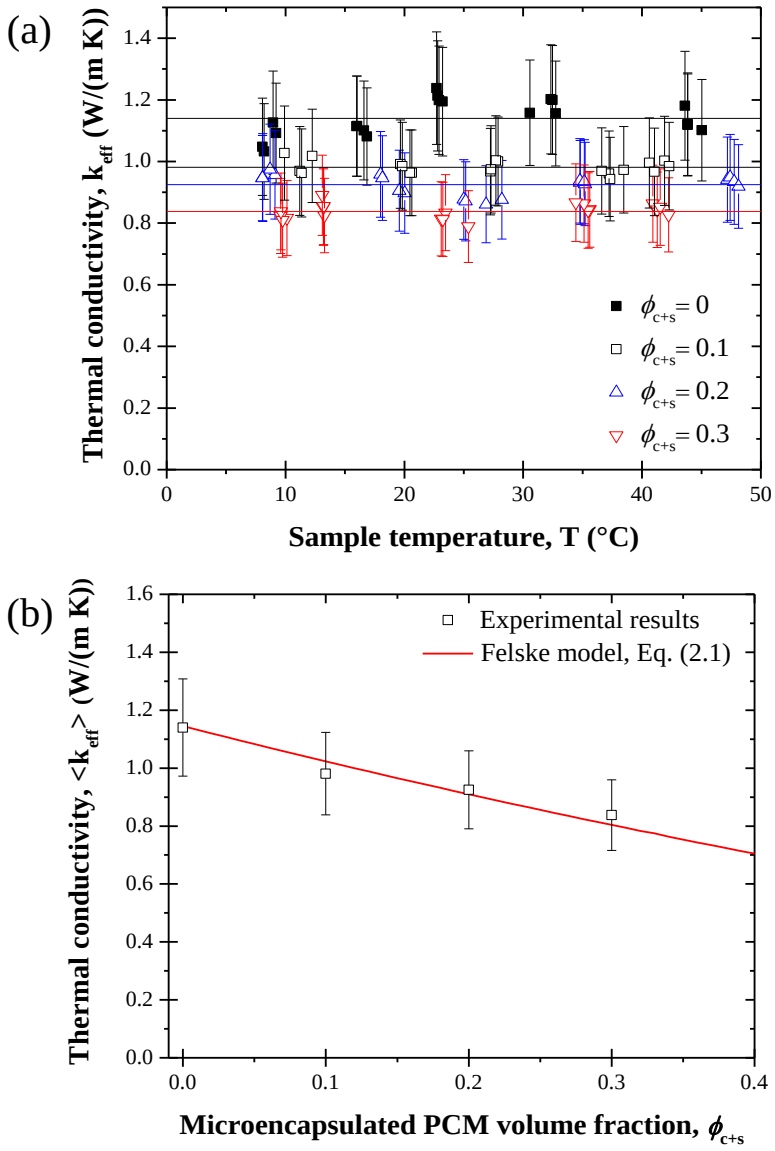

Figure 4.2: (a) Measured effective thermal conductivity k_{eff} of cement paste with a constant w/c ratio of 0.45 and volume fraction of microencapsulated PCM ϕ_{c+s} between 0 and 0.3 as a function of temperature T. (b) Temperature-averaged effective thermal conductivity $<k_{eff}>$ as a function of ϕ_{c+s} with the predictions of the Felske model [13] given by Equation (2.1).

4.3 Cement mortar with microencapsulated PCM

Figure 4.3a plots the effective thermal conductivity k_{eff} of cement mortar containing quartz sand with volume fraction ϕ_q of 0.55, 0.45, and 0.35 as a function of temperature. Similarly, Figure 4.3b plots the effective thermal conductivity k_{eff} of cement mortar containing graded quartz sand with volume fraction ϕ_q and microencapsulated PCM with volume fraction ϕ_{c+s} such that $\phi_q+\phi_{c+s}$=0.55. All samples were aged more than 28 days in ambient air. The error bars correspond to the systematic and random error associated with each measurement, as estimated by Equation (3.11). Figure 4.3 indicates that the thermal conductivity of each cement mortar composite specimen was nearly independent of temperature between 10 and 40°C. Here also, it was not affected appreciably by the occurrence of phase change. Figure 4.3a establishes that the effective thermal conductivity of cement mortar, with constant w/c ratio, increased with increasing quartz sand content. However, Figure 4.3b reveals that for constant volume fraction $\phi_q + \phi_{c+s} = 0.55$, the effective thermal conductivity of cement mortar-PCM composites decreased with increasing PCM volume fraction. Table 4.1 lists the effective thermal conductivity $<k_{eff}>$ averaged over the temperature ranged considered for each composition with various values of ϕ_q and ϕ_{c+s}.

Figure 4.4a plots the ratio $<k_{eff}>/ <k_m>$ of the temperature-averaged effective thermal conductivity of cement mortar-PCM composite specimens $<k_{eff}>$ and the cement mortar $<k_m>$ as a function of microencapsulated PCM volume fraction ϕ_{c+s} ranging from 0 to 0.2. It also shows, in inset, the temperature-averaged thermal conductivity $<k_m>$ as a function of quartz sand volume fraction ϕ_q obtained from data reported in Figure 4.3a. Recall that the volume fraction of the graded quartz sand ϕ_q decreased as microencapsulated PCM was added to maintain the total aggregate volume fraction $\phi_q + \phi_{c+s} = 0.55$. Thus, the effective

matrix thermal conductivity k_m changed as microencapsulated PCM was added. The measured thermal conductivity k_m of cement mortar samples without PCM (i.e., $\phi_{c+s} = 0$) and a graded quartz volume fraction ϕ_q of 0.55, 0.45, and 0.35 was used as the matrix thermal conductivity $<k_m>$ for samples containing ϕ_{c+s} of 0, 0.1, and 0.2, respectively. Figure 4.4a indicates that the thermal conductivity ratio $<k_{eff}>/ <k_m>$ decreased as the microencapsulated PCM volume fraction ϕ_{c+s} increased and the graded quartz sand volume fraction ϕ_q decreased. This can be attributed to the fact that the thermal conductivities of the PCM core and shell were smaller than that of cement mortar. Figure 4.4a also shows predictions by the Felske model [13], given by Equation (2.1). It shows that the predicted thermal conductivity ratio $<k_{eff}>/ <k_m>$ decreased nearly linearly as the microencapsulated PCM volume fraction increased. Here also, predictions by the Felske model [13] for cement mortar-PCM composites agreed very well with experimental results.

Figure 4.4b plots the measured effective thermal conductivity $<k_{eff}>$ of cement mortar-PCM composite specimens as a function of the volume fraction ratio of microencapsulated PCM to total aggregate inclusions $\phi_{c+s}/(\phi_{c+s} + \phi_q)$ ranging from 0 to 0.4. It indicates that the effective thermal conductivity decreased nearly linearly as the microencapsulated PCM volume fraction ϕ_{c+s} increased and $\phi_{c+s}/(\phi_{c+s} + \phi_q)$ increased. Figure 4.4b also shows predictions by the combination of EMA proposed by Brailsford and Major [40] and Park et al. [39], given by Equations (2.2) and (2.3). The randomly oriented graded quartz sand grains were assumed to have an effective thermal conductivity k_q of 7.4 W/(m·K) at room temperature [30]. This was estimated by the weighted geometric mean of the parallel $k_{q,\parallel}$ and perpendicular $k_{q,\perp}$ to the c-axis componts of the anisotropic thermal conductivity of quartz such that $k_q = k_{q,\parallel}^{1/3} k_{q,\perp}^{2/3}$ [60]. Figure 4.4b illustrates that the predictions of EMAs [39, 40] predicted the proper trend but fell

within 26% of the experimental measurements.

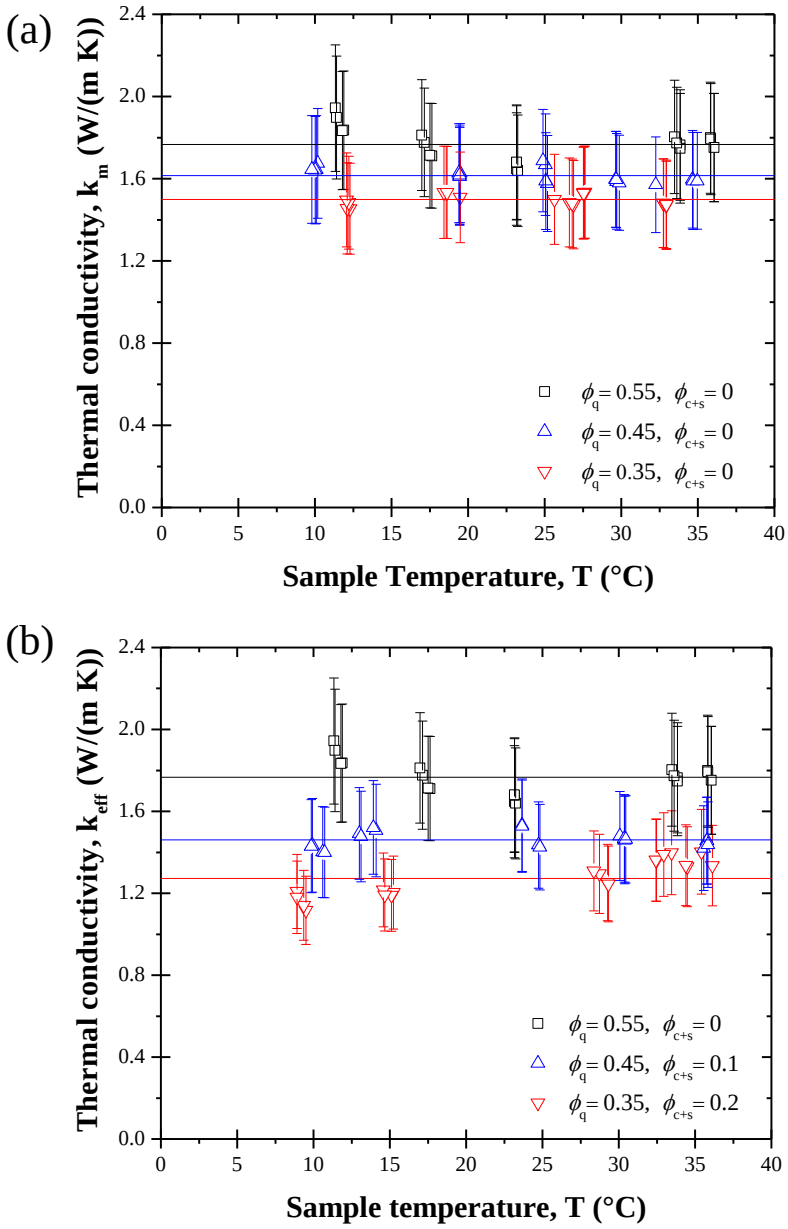

Figure 4.3: Measured effective thermal conductivity of cement mortar with a constant w/c of 0.45 with (a) volume fraction of graded quartz sand ϕ_q between 0.35 and 0.55 and (b) volume fraction of microencapsulated PCM ϕ_{c+s} between 0 and 0.3 and graded quartz sand ϕ_q between 0.35 and 0.55 such that ϕ_q+ϕ_{c+s}=0.55, both as a functions of temperature T.

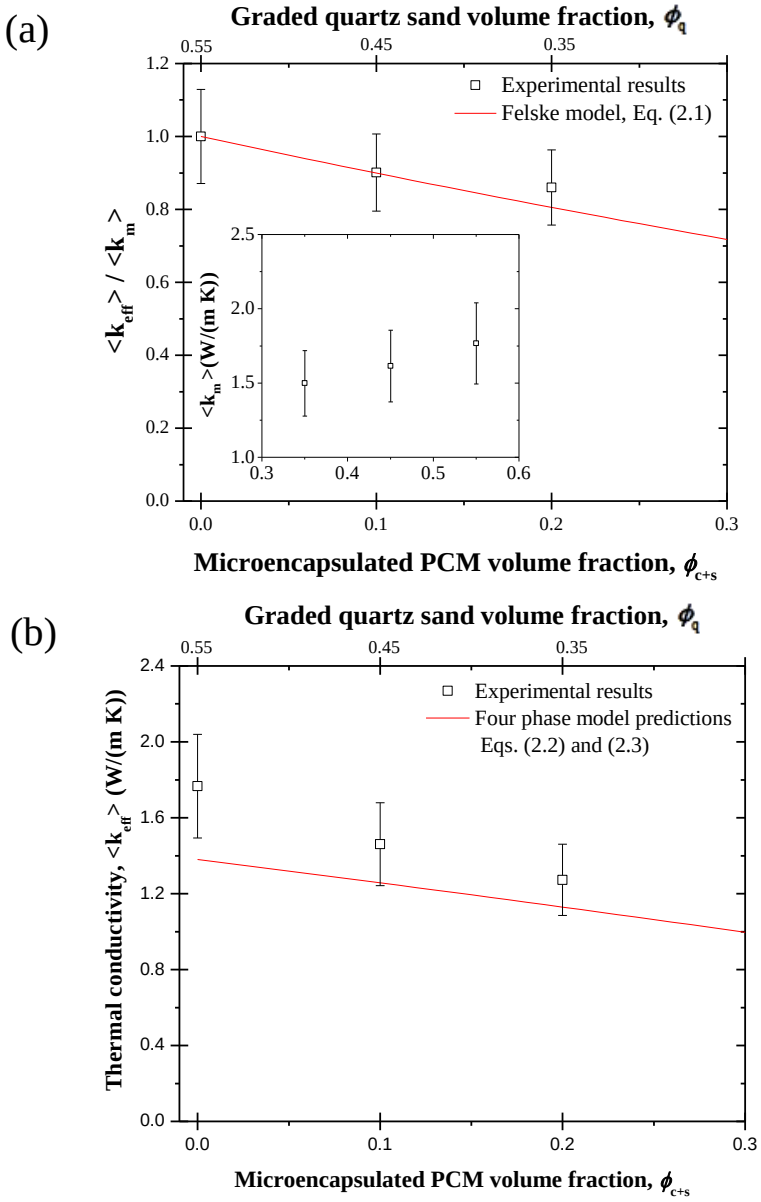

Figure 4.4: (a) Ratio of measured temperature-averaged thermal conductivity $<k_{eff}>/ <k_m>$ of cement mortar with constant w/c of 0.45 as a function of volume fraction of microencapsulated PCM ϕ_{c+s} between 0 and 0.3 for graded quartz sand volume fraction ϕ_q such that $\phi_q + \phi_{c+s} = 0.55$. Here, $<k_m(\phi_q)>$ is shown in the inset and corresponds to temperature-averaged data shown in Figure 4.3a. (b) Comparisons of measured temperature-averaged effective thermal conductivity k_{eff} and predictions of the Brailsford and Major and Park models [39, 40].

Table 4.1: Measured temperature-averaged effective thermal conductivity $<k_{eff}>$ of cement paste and cement mortar samples with microencapsualted PCM volume fraction ϕ_{c+s} ranging from 0 to 0.3. Cement mortar samples had a constant volume fraction of graded quartz sand ϕ_q such that $\phi_q + \phi_{c+s} = 0.55$.

Material	ϕ_{c+s}	ϕ_q	**Temp. range**	ρ_{eff} (g/cm^3)	ρ_{dry} (g/cm^3)	ρ_{sat} (g/cm^3)	ϕ_w	$<k_{eff}>$ (W/(m·K))
	0	0	10 - 40˚C	1.70 ±0.09	1.59	1.96	0.31	1.20 ±0.13
Cement paste	0.10	0	10 - 40˚C	1.57 ±0.08	1.49	1.85	0.21	0.98 ±0.08
and PCM	0.20	0	10 - 40˚C	1.51 ±0.08	1.43	1.65	0.36	0.92 ±0.10
	0.30	0	10 - 40˚C	1.38 ±0.07	1.30	1.50	0.40	0.84 ±0.09
	0	0.55	10 - 40˚C	2.12 ±0.11	2.11	2.29	0.03	1.77 ±0.25
Cement	0	0.45	10 - 40˚C	2.09 ±0.11	2.08	2.20	0.05	1.62 ±0.19
mortar and	0	0.35	10 - 40˚C	1.87 ±0.10	1.86	2.02	0.09	1.50 ±0.10
PCM	0.10	0.45	10 - 40˚C	1.75 ±0.09	1.75	1.93	0.03	1.46 ±0.25
	0.20	0.35	10 - 40˚C	1.71 ±0.09	1.68	1.80	0.26	1.29 ±0.25

CHAPTER 5

Conclusion

A guarded hot plate apparatus was designed, assembled, and validated to measure the effective thermal conductivity of (i) cement paste and (ii) cement mortar containing microencapsulated PCM with volume fraction ϕ_{c+s} of up to 0.3 for temperatures between 10 and 40°C. Cement paste and cement mortar samples were prepared with a constant water to cement ratio of 0.45 and aged for at least 28 days in ambient air. The cement mortar samples included volume fractions ϕ_q of graded quartz sand and ϕ_{c+s} of microencapsulated PCM such that $\phi_q + \phi_{c+s} = 0.55$. The effective density ρ_{eff} and free moisture content ϕ_w of all aged samples were systematically measured. For both composite types, thermal conductivity decreased as the microencapsulated PCM volume fraction increased. For all samples, the thermal conductivity remained nearly constant between $10 - 40$°C. Predictions of the effective medium approximation proposed by Felske [13] for the effective thermal conductivity of core-shell-matrix composites agreed very well with experimental measurements.

Appendix A: Thermal conductivity measurements of composite samples

Material	ϕ_{c+s}	ϕ_q	**Temperature range**	k_{eff} (W/(m·K))
Cement paste	0	0	8.1°C	1.05±0.10
	0	0	8.2°C	1.03±0.10
	0	0	9.0°C	1.13±0.12
	0	0	9.2°C	1.09±0.12
	0	0	16.0°C	1.12±0.10
	0	0	16.0°C	1.12±0.10
	0	0	16.6°C	1.10±0.09
	0	0	16.9°C	1.08±0.09
	0	0	22.8°C	1.21±0.14
	0	0	22.9°C	1.20±0.12
	0	0	23.0°C	1.22±0.15
	0	0	23.2°C	1.19±0.14
	0	0	31.8°C	1.15±0.14
	0	0	32.3°C	1.20±0.11
	0	0	32.5°C	1.20±0.12
	0	0	32.7°C	1.15±0.13
	0	0	41.6°C	1.19±0.14
	0	0	43.6°C	1.18±0.14
	0	0	43.8°C	1.12±0.10
	0	0	45.0°C	1.10±0.13

Material	ϕ_{c+s}	ϕ_q	**Temperature range**	k_{eff} (W/(m·K))
Cement paste	0.1	0	9.9˚C	1.03±0.12
	0.1	0	11.2˚C	0.97±0.16
	0.1	0	11.4˚C	0.96±0.16
	0.1	0	12.2˚C	1.02±0.12
	0.1	0	19.7˚C	0.99±0.06
	0.1	0	19.8˚C	0.99±0.06
	0.1	0	20.5˚C	0.96±0.06
	0.1	0	20.6˚C	0.96±0.06
	0.1	0	27.2˚C	0.97±0.09
	0.1	0	27.3˚C	0.97±0.09
	0.1	0	27.2˚C	1.00±0.06
	0.1	0	27.9˚C	1.00±0.06
	0.1	0	36.6˚C	0.97±0.06
	0.1	0	37.2˚C	0.96±0.06
	0.1	0	37.3˚C	0.94±0.06
	0.1	0	38.5˚C	0.97±0.06
	0.1	0	40.6˚C	0.99±0.10
	0.1	0	41.1˚C	0.97±0.09
	0.1	0	41.9˚C	1.00±0.06
	0.1	0	42.3˚C	0.99±0.06

Material	ϕ_{c+s}	ϕ_q	**Temperature range**	k_{eff} (W/(m·K))
Cement paste	0.2	0	8.0˚C	0.95±0.14
	0.2	0	8.1˚C	0.95±0.14
	0.2	0	8.7˚C	0.98±0.13
	0.2	0	9.1˚C	0.96±0.13
	0.2	0	18.0˚C	0.96±0.08
	0.2	0	18.1˚C	0.95±0.08
	0.2	0	19.6˚C	0.91±0.07
	0.2	0	20.0˚C	0.90±0.07
	0.2	0	25.7˚C	0.91±0.09
	0.2	0	26.9˚C	0.86±0.07
	0.2	0	27.9˚C	0.90±0.08
	0.2	0	28.2˚C	0.88±0.08
	0.2	0	34.8˚C	0.94±0.06
	0.2	0	34.8˚C	0.94±0.06
	0.2	0	35.2˚C	0.93±0.08
	0.2	0	35.2˚C	0.94±0.08
	0.2	0	47.2˚C	0.94±0.09
	0.2	0	47.4˚C	0.95±.09
	0.2	0	47.8˚C	0.94±0.10
	0.2	0	48.1˚C	0.92±0.09

Material	ϕ_{c+s}	ϕ_q	**Temperature range**	k_{eff} (W/(m·K))
Cement paste	0.3	0	9.6˚C	0.84±0.11
	0.3	0	9.6˚C	0.82±0.12
	0.3	0	9.7˚C	0.81±0.10
	0.3	0	10.1˚C	0.82±0.11
	0.3	0	13.1˚C	0.89±0.08
	0.3	0	13.2˚C	0.85±0.07
	0.3	0	13.2˚C	0.85±0.07
	0.3	0	13.3˚C	0.85±0.07
	0.3	0	23.1˚C	0.82±0.11
	0.3	0	23.2˚C	0.81±0.12
	0.3	0	23.5˚C	0.84±0.11
	0.3	0	25.4˚C	0.79±0.11
	0.3	0	34.4˚C	0.87±0.07
	0.3	0	35.1˚C	0.86±0.07
	0.3	0	35.5˚C	0.84±0.07
	0.3	0	35.6˚C	0.85±0.07
	0.3	0	40.9˚C	0.86±0.07
	0.3	0	41.3˚C	0.84±0.07
	0.3	0	41.5˚C	0.85±0.07
	0.3	0	42.2˚C	0.83±0.07

Material	ϕ_{c+s}	ϕ_q	**Temperature range**	k_{eff} (W/(m·K))
Cement mortar	0	0.55	11.3˚C	1.93±0.37
	0	0.55	11.4˚C	1.88±0.36
	0	0.55	11.8˚C	1.82±0.33
	0	0.55	11.9˚C	1.82±0.33
	0	0.55	17.0˚C	1.82±0.21
	0	0.55	17.1˚C	1.78±0.21
	0	0.55	17.5˚C	1.72±0.23
	0	0.55	17.6˚C	1.72±0.23
	0	0.55	23.2˚C	1.70±0.28
	0	0.55	23.2˚C	1.70±0.28
	0	0.55	23.2˚C	1.66±0.29
	0	0.55	23.2˚C	1.67±0.29
	0	0.55	33.5˚C	1.80±0.21
	0	0.55	33.6˚C	1.77±0.21
	0	0.55	33.8˚C	1.76±0.21
	0	0.55	33.8˚C	1.74±0.21
	0	0.55	35.8˚C	1.80±0.19
	0	0.55	35.8˚C	1.80±0.19
	0	0.55	36.1˚C	1.76±0.18
	0	0.55	36.1˚C	1.76±0.18

Material	ϕ_{c+s}	ϕ_q	**Temperature range**	k_{eff} (W/(m·K))
Cement mortar	0	0.45	9.8˚C	1.64±0.28
	0	0.45	10.0˚C	1.63±0.28
	0	0.45	10.1˚C	1.64±0.27
	0	0.45	10.2˚C	1.67±0.29
	0	0.45	19.4˚C	1.63±0.19
	0	0.45	19.5˚C	1.63±0.19
	0	0.45	19.5˚C	1.61±0.19
	0	0.45	19.5˚C	1.62±0.19
	0	0.45	24.9˚C	1.69±0.14
	0	0.45	25.1˚C	1.59±0.17
	0	0.45	25.1˚C	1.67±0.14
	0	0.45	25.2˚C	1.58±0.17
	0	0.45	29.6˚C	1.60±0.14
	0	0.45	29.7˚C	1.59±0.12
	0	0.45	29.7˚C	1.60±0.12
	0	0.45	29.9˚C	1.58±0.12
	0	0.45	32.2˚C	1.57±0.19
	0	0.45	34.7˚C	1.60±0.21
	0	0.45	34.7˚C	1.59±0.19
	0	0.45	35.0˚C	1.59±0.19

Material	ϕ_{c+s}	ϕ_q	**Temperature range**	k_{eff} (W/(m·K))
Cement mortar	0	0.35	12.1˚C	1.45±0.17
	0	0.35	12.1˚C	1.49±0.17
	0	0.35	12.2˚C	1.48±0.17
	0	0.35	12.3˚C	1.45±0.16
	0	0.35	18.4˚C	1.53±0.11
	0	0.35	18.6˚C	1.53±0.11
	0	0.35	18.6˚C	1.53±0.11
	0	0.35	19.5˚C	1.51±0.11
	0	0.35	25.6˚C	1.50±0.10
	0	0.35	26.6˚C	1.48±0.10
	0	0.35	26.8˚C	1.48±0.10
	0	0.35	26.9˚C	1.47±0.10
	0	0.35	27.5˚C	1.53±0.10
	0	0.35	27.5˚C	1.53±0.10
	0	0.35	27.6˚C	1.53±0.10
	0	0.35	27.6˚C	1.53±0.10
	0	0.35	32.7˚C	1.48±0.09
	0	0.35	32.8˚C	1.48±0.09
	0	0.35	32.9˚C	1.47±0.09
	0	0.35	33.0˚C	1.47±0.09

Material	ϕ_{c+s}	ϕ_q	**Temperature range**	k_{eff} (W/(m·K))
Cement mortar	0.1	0.45	9.9°C	1.44±0.22
	0.1	0.45	9.9°C	1.43±0.22
	0.1	0.45	10.6°C	1.40±0.19
	0.1	0.45	10.7°C	1.40±0.19
	0.1	0.45	13.0°C	1.49±0.20
	0.1	0.45	13.1°C	1.47±0.20
	0.1	0.45	13.9°C	1.49±0.20
	0.1	0.45	14.1°C	1.50±0.21
	0.1	0.45	23.7°C	1.53±0.17
	0.1	0.45	23.7°C	1.53±0.17
	0.1	0.45	24.8°C	1.44±0.16
	0.1	0.45	24.8°C	1.43±0.15
	0.1	0.45	30.1°C	1.48±0.13
	0.1	0.45	30.4°C	1.46±0.13
	0.1	0.45	30.4°C	1.47±0.10
	0.1	0.45	30.5°C	1.46±0.10
	0.1	0.45	35.6°C	1.42±0.09
	0.1	0.45	35.8°C	1.46±0.09
	0.1	0.45	35.8°C	1.46±0.09
	0.1	0.45	35.8°C	1.44±0.09

Material	ϕ_{c+s}	ϕ_q	**Temperature range**	k_{eff} (W/(m·K))
Cement mortar	0.2	0.35	8.9°C	1.18±0.15
	0.2	0.35	8.9°C	1.21±0.15
	0.2	0.35	9.4°C	1.14±0.15
	0.2	0.35	9.5°C	1.12±0.15
	0.2	0.35	14.6°C	1.22±0.13
	0.2	0.35	14.7°C	1.19±0.13
	0.2	0.35	15.1°C	1.19±0.11
	0.2	0.35	15.2°C	1.20±0.11
	0.2	0.35	28.4°C	1.31±0.14
	0.2	0.35	28.7°C	1.30±0.13
	0.2	0.35	29.3°C	1.25±0.12
	0.2	0.35	29.3°C	1.25±0.12
	0.2	0.35	32.4°C	1.36±0.12
	0.2	0.35	32.5°C	1.36±0.12
	0.2	0.35	32.9°C	1.39±0.12
	0.2	0.35	33.5°C	1.40±0.12
	0.2	0.35	34.4°C	1.34±0.15
	0.2	0.35	34.5°C	1.33±0.14
	0.2	0.35	35.4°C	1.40±0.14
	0.2	0.35	36.1°C	1.34±0.13

Appendix B: Thermal conductivity of CRM Pyrex 7740 samples

Material	**Temperature**	k_{exp} (W/(m·K))	k_p**(T)** (W/(m·K))
Pyrex 7740	9.2˚C	1.18±0.17	1.12
	9.3˚C	1.18±0.17	1.12
	9.7˚C	1.19±0.15	1.12
	9.9˚C	1.18±0.15	1.12
	22.1˚C	1.16±0.13	1.14
	22.2˚C	1.16±0.13	1.14
	28.6˚C	1.18±0.10	1.15
	29.1˚C	1.10±0.15	1.15
	29.2˚C	1.09±0.16	1.15
	29.2˚C	1.15±0.15	1.15
	29.2˚C	1.06±0.15	1.15
	29.4˚C	1.07±0.15	1.15
	30.1˚C	1.11±0.13	1.15
	30.2˚C	1.12±0.14	1.15
	30.7˚C	1.17±0.17	1.15
	30.8˚C	1.20±0.17	1.15
	31.5˚C	1.12±0.14	1.15

Material	**Temperature**	k_{exp} (W/(m·K))	k_p**(T)** (W/(m·K))
Pyrex 7740	32.1°C	1.07±0.12	1.16
	32.5°C	1.15±0.14	1.16
	33.2°C	1.16±0.13	1.16
	38.0°C	1.17±0.14	1.17
	38.7°C	1.11±0.13	1.17

References

[1] F. Kuznik, D. David, K. Johannes, and J.-J. Roux, "A review on phase change materials integrated in building walls", *Renewable and Sustainable Energy Reviews*, vol. 15, no. 1, pp. 379–391, 2011.

[2] T.-C. Ling and C.-S. Poon, "Use of phase change materials for thermal energy storage in concrete: An overview", *Construction and Building Materials*, vol. 46, pp. 55–62, 2013.

[3] M.K. Rathod and J. Banerjee, "Thermal stability of phase change materials used in latent heat energy storage systems: a review", *Renewable and Sustainable Energy Reviews*, vol. 18, pp. 246–258, 2013.

[4] F. Fernandes, S. Manari, M. Aguayo, K. Santos, T. Oey, Z. Wei, G. Falzone, N. Neithalath, and G. Sant, "On the feasibility of using phase change materials (pcms) to mitigate thermal cracking in cementitious materials", *Cement and Concrete Composites*, vol. 51, pp. 14–26, 2014.

[5] D.P. Bentz and R. Turpin, "Potential applications of phase change materials in concrete technology", *Cement and Concrete Composites*, vol. 29, no. 7, pp. 527–532, 2007.

[6] L.F. Cabeza, C. Castellon, M. Nogues, M. Medrano, R. Leppers, and O. Zubillaga, "Use of microencapsulated PCM in concrete walls for energy savings", *Energy and Buildings*, vol. 39, no. 2, pp. 113–119, 2007.

[7] D. Zhou, C.-Y. Zhao, and Y. Tian, "Review on thermal energy storage with phase change materials (PCMs) in building applications", *Applied Energy*, vol. 92, pp. 593–605, 2012.

[8] M. Hunger, A.G. Entrop, I. Mandilaras, H.J.H. Brouwers, and M. Founti, "The behavior of self-compacting concrete containing micro-encapsulated phase change materials", *Cement and Concrete Composites*, vol. 31, no. 10, pp. 731–743, 2009.

[9] A. Sharma, V.V. Tyagi, C.R. Chen, and D. Buddhi, "Review on thermal energy storage with phase change materials and applications", *Renewable and Sustainable Energy Reviews*, vol. 13, no. 2, pp. 318–345, 2009.

[10] V.V. Tyagi, S.C. Kaushik, S.K. Tyagi, and T. Akiyama, "Development of phase change materials based microencapsulated technology for buildings: a review", *Renewable and Sustainable Energy Reviews*, vol. 15, no. 2, pp. 1373–1391, 2011.

[11] A.M. Thiele, G. Sant, and L. Pilon, "Diurnal thermal analysis of microencapsulated PCM-concrete composite walls", *Energy Conversion and Management*, vol. 93, pp. 215–227, 2015.

[12] A.M. Thiele, A. Jamet, G. Sant, and L. Pilon, "Annual energy analysis of concrete containing phase change materials for building envelopes", *Energy Conversion and Management*, vol. 103, pp. 374–386, 2015.

[13] J.D. Felske, "Effective thermal conductivity of composite spheres in a continuous medium with contact resistance", *International Journal of Heat and Mass Transfer*, vol. 47, no. 14, pp. 3453–3461, 2004.

[14] T. Log and S.E. Gustafsson, "Transient plane source (TPS) technique for measuring thermal transport properties of building materials", *Fire and Materials*, vol. 19, no. 1, pp. 43–49, 1995.

[15] S.E. Gustafsson, "Transient hot strip techniques for measuring thermal conductivity and thermal diffusivity", *The Rigaku Journal*, vol. 4, no. 1/2, pp. 16–28, 1987.

[16] J.J. Healy, J.J. De Groot, and J. Kestin, "The theory of the transient hot-wire method for measuring thermal conductivity", *Physica B & C*, vol. 82, no. 2, pp. 392–408, 1976.

[17] U. Hammerschmidt and V. Meier, "New transient hot-bridge sensor to measure thermal conductivity, thermal diffusivity, and volumetric specific heat", *International Journal of Thermophysics*, vol. 27, no. 3, pp. 840–865, 2006.

[18] W.J. Parker, R.J. Jenkins, C.P. Butler, and G.L. Abbott, "Flash method of determining thermal diffusivity, heat capacity, and thermal conductivity", *Journal of Applied Physics*, vol. 32, no. 9, pp. 1679–1684, 1961.

[19] D. Kuvandykova and R. St-Laurent, "Application of the modified transient plane source technique in testing the thermal conductivity of concrete", *C-Therm Technol*, vol. 18, pp. 1–7, 2010.

[20] P.S. Gaal, M.-A. Thermitus, and D.E. Stroe, "Thermal conductivity measurements using the flash method", *Journal of Thermal Analysis and Calorimetry*, vol. 78, no. 1, pp. 185–189, 2004.

[21] C. Bankvall, "Guarded hot plate apparatus for the investigation of thermal insulations", *Matériaux et Construction*, vol. 6, no. 1, pp. 39–47, 1973.

[22] D. Salmon, "Thermal conductivity of insulations using guarded hot plates, including recent developments and sources of reference materials", *Measurement Science and Technology*, vol. 12, no. 12, pp. R89, 2001.

[23] ASTM Standard, "C177-13", *Standard test method for steady-state heat flux measurements and thermal transmission properties by means of the guarded-hot plate apparatus. ASTM International, West Conshohocken, PA, USA*, 2014.

[24] D.P. Bentz, "Transient plane source measurements of the thermal properties of hydrating cement pastes", *Materials and Structures*, vol. 40, no. 10, pp. 1073–1080, 2007.

[25] Y. Xu and D.D.L. Chung, "Increasing the specific heat of cement paste by admixture surface treatments", *Cement and Concrete Research*, vol. 29, no. 7, pp. 1117–1121, 1999.

[26] Y. Xu and D.D.L. Chung, "Effect of sand addition on the specific heat and thermal conductivity of cement", *Cement and Concrete Research*, vol. 30, no. 1, pp. 59–61, 2000.

[27] R. Demirboğa, "Thermal conductivity and compressive strength of concrete incorporation with mineral admixtures", *Building and Environment*, vol. 42, no. 7, pp. 2467–2471, 2007.

[28] M.I. Khan, "Factors affecting the thermal properties of concrete and applicability of its prediction models", *Building and Environment*, vol. 37, no. 6, pp. 607–614, 2002.

[29] D. Campbell-Allen and C.P. Thorne, "The thermal conductivity of concrete", *Magazine of Concrete Research*, vol. 15, no. 43, pp. 39–48, 1963.

[30] T.L. Bergman, A.S. Lavine, F.P. Incropera, and D.P. DeWitt, *Fundamentals of Heat and Mass Transfer*, John Wiley & Sons, New York City, NY, 7^{th} edition, 2011.

[31] K. Liu, Z. Wang, C. Jin, F. Wang, and X. Lu, "An experimental study on thermal conductivity of iron ore sand cement mortar", *Construction and Building Materials*, vol. 101, pp. 932–941, 2015.

[32] T.D. Brown and M.Y. Javaid, "The thermal conductivity of fresh concrete", *Matériaux et Construction*, vol. 3, no. 6, pp. 411–416, 1970.

[33] G. De Schutter and L. Taerwe, "Specific heat and thermal diffusivity of hardening concrete", *Magazine of Concrete Research*, vol. 47, no. 172, pp. 203–208, 1995.

[34] K.H. Kim, S.E. Jeon, J.K. Kim, and S. Yang, "An experimental study on thermal conductivity of concrete", *Cement and Concrete Research*, vol. 33, no. 3, pp. 363–371, 2003.

[35] H. Uysal, R. Demirboğa, R. Şahin, and R. Gül, "The effects of different cement dosages, slumps, and pumice aggregate ratios on the thermal conductivity and density of concrete", *Cement and Concrete Research*, vol. 34, no. 5, pp. 845–848, 2004.

[36] H.-Q. Jin, X.-L. Yao, L.-W. Fan, X. Xu, and Z.-T. Yu, "Experimental determination and fractal modeling of the effective thermal conductivity of autoclaved aerated concrete: Effects of moisture content", *International Journal of Heat and Mass Transfer*, vol. 92, pp. 589–602, 2016.

[37] B. Xu and Z. Li, "Paraffin/diatomite composite phase change material incorporated cement-based composite for thermal energy storage", *Applied Energy*, vol. 105, pp. 229–237, 2013.

[38] Z. Zhang, G. Shi, S. Wang, X. Fang, and X. Liu, "Thermal energy storage cement mortar containing n-octadecane/expanded graphite composite phase change material", *Renewable Energy*, vol. 50, pp. 670–675, 2013.

[39] Y.K. Park, J.G. Kim, and J.K. Lee, "Prediction of thermal conductivity of composites with spherical microballoons", *Materials Transactions*, vol. 49, no. 12, pp. 2781–2785, 2008.

[40] A.D. Brailsford and K.G. Major, "The thermal conductivity of aggregates of several phases, including porous materials", *British Journal of Applied Physics*, vol. 15, no. 3, pp. 313, 1964.

[41] M. Porfiri, N.Q. Nguyen, and N. Gupta, "Thermal conductivity of multiphase particulate composite materials", *Journal of Materials Science*, vol. 44, no. 6, pp. 1540–1550, 2009.

[42] W.M.J.H. Woodside and J.H. Messmer, "Thermal conductivity of porous media. I. Unconsolidated sands", *Journal of Applied Physics*, vol. 32, no. 9, pp. 1688–1699, 1961.

[43] T. Zakri, J.P. Laurent, and M. Vauclin, "Theoretical evidence for Lichtenecker's mixture formulae based on the effective medium theory", *Journal of Physics D: Applied Physics*, vol. 31, no. 13, pp. 1589, 1998.

[44] A.M. Thiele, A. Kumar, G. Sant, and L. Pilon, "Effective thermal conductivity of three-component composites containing spherical capsules", *International Journal of Heat and Mass Transfer*, vol. 73, pp. 177–185, 2014.

[45] ASTM Standard, "C305", *Standard practice for mechanical mixing of hydraulic cement pastes and mortars of plastic consistency. ASTM International, West Conshohocken, PA, USA*, 2014.

[46] "MPCM Technical Information", Tech. Rep., Microtek Laboratories Inc., Dayton, OH.

[47] A.M. Thiele, Z. Wei, G. Falzone, B. Young, N. Niethalath, G. Sant, and L. Pilon, "Figure of merit for the thermal performance of cementitious composites containing phase change materials", *Cement and Concrete Composites*, vol. 65, no. 1, pp. 214–226, 2016.

[48] ASTM Standard, "C788-06", *Standard specification for standard sand. ASTM International, West Conshohocken, PA, USA*, 2006.

[49] T.L. Youd, "Factors controlling maximum and minimum densities of sands", *ASTM Special Technical Publications*, vol. 523, pp. 98–112, 1973.

[50] Z. Lafhaj, M. Goueygou, A. Djerbi, and M. Kaczmarek, "Correlation between porosity, permeability and ultrasonic parameters of mortar with variable water/cement ratio and water content", *Cement and Concrete Research*, vol. 36, no. 4, pp. 625–633, 2006.

[51] "Cerablanket, Cerachem, Cerachrome Blanket datasheet", Tech. Rep., Morgan Thermal Ceramics, Inc., Windsor, Berkshire, United Kingdom.

[52] "Dynalene HC Series", Tech. Rep., Dynalene Inc., Whitehall, PA.

[53] U. Hammerschmidt, "Guarded hot-plate (GHP) method: Uncertainty assessment", *International Journal of Thermophysics*, vol. 23, no. 6, pp. 1551–1570, 2002.

[54] H. Simmler, "Uncertainty assessment of guarded hot plate apparatus", Tech. Rep., EMPA Building Technologies Lab, Düebendorf, Switzerland, June 2008.

[55] S.L. Meyers, "Thermal expansion characteristics of hardened cement paste and of concrete", in *Highway Research Board Proceedings*, 1951, vol. 30, pp. 193–203.

[56] E.J. Sellevold and Ø. Bjøntegaard, "Coefficient of thermal expansion of cement paste and concrete: Mechanisms of moisture interaction", *Materials and Structures*, vol. 39, no. 9, pp. 809–815, 2006.

[57] BCR Certified reference material, "BCR-039", *Certified reference material BCR-039, Pyrex Glass. Institue for Reference Materials and Measurements, European Union*, 2007.

[58] N. Ukrainczyk, S. Kurajica, and J. Šipušić, "Thermophysical comparison of five commercial paraffin waxes as latent heat storage materials", *Chemical and Biochemical Engineering Quarterly*, vol. 24, no. 2, pp. 129–137, 2010.

[59] R.K. Rajput, *Engineering Materials & Metallurgy*, S. Chand Publishing Limited, New Delhi, India, 1st edition, 2006.

[60] V.R. Tarnawski, T. Momose, W.H. Leong, G. Bovesecchi, and P. Coppa, "Thermal conductivity of standard sands. part I. Dry-state conditions", *International Journal of Thermophysics*, vol. 30, no. 3, pp. 949–968, 2009.